portant in the regulation of intracellular Ca^{2+} homeostasis and its expression is induced under conditions of troubled homeostasis, including ER stress (Osman et al., 2003; Yamaguchi et al., 2004; Ueda et al., 2005; Takei et al., 2006). In addition, mutation screening analyses in Wolfram syndrome patients showed more than 50 distinct mutations of the *WFS1* gene, including stop, frameshift, deletion, and missense mutations (Inoue et al., 1998; Strom et al., 1998; Hardy et al., 1999; Gómez-Zaera et al., 2001; Khanim et al., 2001; Tessa et al., 2001). Thus, loss-of-function mutations in the *WFS1* gene have been linked to Wolfram syndrome. However, roles of WFS1 protein in cellular functions and the mechanism by which mutations of the *WFS1* gene cause Wolfram syndrome remain unclear.

The association of diabetes mellitus and optic atrophy has been known since at least 1858 when von Gräfe reported optic atrophy as a complication of diabetes mellitus (von Gräfe, 1858). This report is probably the first description of Wolfram syndrome (Minton et al., 2003). The prevalence of Wolfram syndrome is one per 770,000 in the UK population and the median age of onset of optic atrophy is 11 years (Barrett et al., 1995). The ophthalmologic signs are a progressive decrease in visual acuity, constriction of the peripheral visual field with or without central scotoma, color vision disturbance, and bilateral optic disc atrophy. Diabetic retinopathy is a rare complication (Mtanda et al., 1986; Seynaeve et al., 1994; Barrett et al., 1997). Although a profound reduction in visual function is observed in Wolfram syndrome patients, the electroretinogram (ERG) tests indicate normal or only slightly reduced responses (Niemeyer and Marquardt, 1972; Mtanda et al., 1986; Seynaeve et al., 1994; Barrett et al., 1997). These findings suggest that the site of pathology for optic atrophy lies not in the retina, but in the visual pathway proximal (posterior) to the eye including the optic nerve (Barrett et al., 1997). In addition, brains of Wolfram syndrome patients showed neuronal loss and gliosis in the lateral geniculate nucleus (LGN) and superior colliculus (SC) as well as severe degeneration of the optic nerve (Genís et al., 1997; Shannon et al., 1999). Thus, ophthalmologic and neuropathological facts concerning optic atrophy in Wolfram syndrome have been accumulated. However, the site of pathology, i.e., causative cell types, for the optic atrophy remains unclear. To obtain insights into causative cell types for optic atrophy it is necessary to examine *WFS1* expression not only in the retina but also in the optic nerve, the optic chiasm, the optic tract, and in the retino-recipient nuclei, since there is a possibility that the optic atrophy is due to neuronal loss in the retino-recipient nuclei caused by loss-of-function mutations in the *WFS1* gene (retrograde transsynaptic degeneration). Insights into the causative cell types may provide hypotheses about the pathogenesis of optic atrophy in Wolfram syndrome.

In the rodent central nervous system (CNS), *Wfs1* expression has previously been described in neurons of the cerebral cortex, the basal ganglia, the hypothalamus, the brainstem motor and sensory nuclei, the reticular formation, and the cerebellar cortex, as well as in hippocampal CA1 pyramidal neurons (Takeda et al., 2001, Ishihara et al., 2004). In the visual system, recent studies suggest that WFS1 protein is expressed in retinal ganglion cells (RGCs) and optic nerve glia of the cynomolgus monkey (Yamamoto et al., 2006). To know species differences in the localization of WFS1 protein in the visual system, to obtain insights into causative cell types for optic atrophy in Wolfram syndrome, and to establish a basis for functional studies of WFS1 in the visual system, we performed a detailed histochemical analysis of the distribution of *Wfs1* mRNA and protein in the normal mouse visual system including the retina, the optic nerve, the optic chiasm, the optic tract, the retino-recipient nuclei, and the visual cortex.

MATERIALS AND METHODS

Animals and tissue preparation

Male mice (n = 24; 7–8 weeks old; C57BL/6NCrlCrlj; Charles River Laboratories Japan, Yokohama, Kanagawa, Japan) were used in this study. Seven-week-old mice were used for the retrograde labeling of RGCs and 8-week-old mice for immunoblot and histochemistry.

For immunoblot analysis the mice were deeply anesthetized with sodium pentobarbital (50 mg/kg, i.p.). The brain, retina, and optic nerve were dissected from the skull on ice, immediately frozen in liquid nitrogen, and stored at –70°C prior to use. For histochemistry by using frozen sections the mice were deeply anesthetized with sodium pentobarbital (50 mg/kg, i.p.) and perfused transcardially with 4% paraformaldehyde dissolved in 0.1 M sodium phosphate buffer (PB; pH 7.4) at 4°C. The eyeballs including the optic nerve and the brain were removed from the skull, stored in the same fixative for 48 hours, and then immersed in 30% saccharose in 0.1 M PB at 4°C until they sank. The eyeballs including the optic nerve were frozen in powdered dry ice and sectioned in the meridian plane at a thickness of 25 μm on a cryostat. The brains were frozen and coronally cut at a thickness of 40 μm. The sections were collected in a cryoprotectant medium (33.3% saccharose, 1% polyvinylpyrrolidone (K-30), and 33.3% ethylene glycol in 0.067 M sodium PB (pH 7.4) containing 0.067% sodium azide; Warr et al., 1981) and stored at –30°C prior to use. For immunohistochemistry by using whole-mount retinae the mice were anesthetized and perfused as described above. The eyeballs were removed from the skull and stored in the same fixative for 48 hours. The retina was gently dissected and immersed in 30% saccharose in 0.1 M PB at 4°C until they sank. The retina was shock-frozen in acetone at –70°C and stored in a freezer at the same temperature prior to use.

All experimental protocols for this study were approved by the committees on the Ethics of Animal Experimentation at Kagoshima University or at Yamaguchi University School of Medicine. The protocols were conducted according to the guidelines for Animal Research of Kagoshima University or Yamaguchi University School of Medicine and The Law (No. 105) and Notification (No. 6) of the Japanese Government.

Retrograde labeling of retinal ganglion cells

Seven-week-old mice were anesthetized with a mixture containing ketamine hydrochloride (60 mg/kg, i.p.) and xylazine (6 mg/kg, i.p.). A full-strength solution of Fluorescent Latex Microspheres (Red fluorescent RetroBeads; rhodamine label, Lumafluor, Naples, FL) was stereotaxically injected through a glass micropipette (20–30 μm in tip diameter) by air pressure. The injection was made into the bilateral SC (six mice). After a period of 4 days the mice

were reanesthetized and perfused as described above. In addition, Fluoro-Ruby (dextran-tetramethylrhodamine, Molecular Probes, Eugene, OR) was used as another retrograde tracer. A 10% (w/v) solution dissolved in saline was injected. The injection was made into the bilateral LGN (two mice), the bilateral SC (two mice), or both the bilateral LGN and the bilateral SC (two mice). The survival period was set at 3–5 days. Other procedures were the same as those in the Fluorescent Latex Microspheres injection cases.

Antibodies

Preparation of the affinity-purified rabbit anti-Wfs1 N-terminus (anti-Wfs1) antibody recognizing the N-terminus 179 amino acids of mouse Wfs1 protein was described previously (Cryns et al., 2003). In brief, a cDNA fragment encoding the N-terminal 290 amino acids of mouse Wfs1 was cloned into pGEX-6P-1 plasmid (Amersham Biosciences, Tokyo, Japan) to produce chimeric proteins consisting of the N-terminal sequence of Wfs1 (1–290) and the C-terminal glutathione *S*-transferase (GST) protein, termed GST-Wfs1N. The cDNA encoding the N-terminal 179 amino acids of mouse Wfs1 was also cloned into the pMAL-c2 plasmid (New England Biolabs, Ipswich, MA) to produce a fusion protein consisting of the N-terminal sequence of mouse Wfs1 and maltose-binding protein (MBP), termed Wfs1N-MBP. The GST-Wfs1N and Wfs1N-MBP chimeric proteins were expressed in *Escherichia coli* (JM109 strain) and induced by 1 mM isopropyl-thiogalactopyranoside (IPTG). Bacterial lysates were mixed with glutathione Sepharose 4B (Amersham Biosciences) and amylose resin (New England Biolabs) for purification of GST-Wfs1N and Wfs1N-MBP. The bound GST-Wfs1N chimeric protein was eluted from glutathione Sepharose 4B by addition of 10 mM reduced glutathione solution. The eluted GST-Wfs1N chimeric protein was used for immunizing Japanese White rabbits. Rabbit antisera were collected and affinity-purified by using Wfs1N-MBP bound to the amylose resin.

The following antibodies were obtained from commercial suppliers and applied in order to label specific cell types of the retina and optic nerve. Horizontal cells and nondisplaced amacrine cells were immunolabeled with a mouse monoclonal antibody against calbindin-D-28K (Haverkamp and Wässle, 2000). Rod and (putative) ON-cone bipolar cells were immunostained with a mouse monoclonal antibody against G-protein Goα (Haverkamp and Wässle, 2000). Cholinergic amacrine cells were labeled with a goat polyclonal antibody against choline acetyltransferase (ChAT) (Jeon et al., 1998; Haverkamp and Wässle, 2000; Kang et al., 2004). RGCs including their dendrites and axons were immunolabeled with a mouse monoclonal antibody against tubulin, βIII isoform (Sharma and Netland, 2007). According to the criteria of Sharma and Netland (2007), large cells intensely labeled with this antibody in the GCL were recognized as RGCs. Nuclei of RGCs were immunostained with a mouse monoclonal antibody against Brn-3a POU-domain transcription factor (Xiang et al., 1995). Müller cells and glial cells in the optic nerve were labeled with a mouse monoclonal antibody against glutamine synthetase (Haverkamp and Wässle, 2000). Astrocytes were immunolabeled with a rabbit serum or a mouse monoclonal antibody against glial fibrillary acidic protein (GFAP) (Morcos and Chan-Ling, 2000). As for the anti-GFAP rabbit serum, this serum stains a single protein band of 51 kDa in the mouse brain on immunoblot (Jalil et al., 2005). Oligodendrocytes were immunostained with a mouse monoclonal antibody against oligodendrocytes [RIP] (Friedman et al., 1989). Specificity of this antibody was strictly verified in the rat CNS (Friedman et al., 1989). In the rat cerebellum, strong RIP staining was mainly confined to the white matter, although moderate RIP staining was distributed in the granular layer. In the molecular layer, composed of the unmyelinated parallel fibers, RIP staining was hardly detected (Friedman et al., 1989). In the mouse cerebellum the staining pattern of this antibody (data not shown) was identical to that in the rat cerebellum. In the mouse optic nerve the staining pattern was also identical to that in the rat (Saari et al., 1997; Morcos and Chan-Ling, 2000). Microglia were labeled with a rat monoclonal antibody against mouse CD11b (Mac-1 α chain) (Dräger, 1983; Reichert and Rotshenker, 1996). The staining patterns of these antibodies were identical to those previously published and their source, host species, antigen, and specificity are listed in Table 1.

Immunoblot analysis

The tissue of the brain, retina, and optic nerve was homogenized in phosphate-buffered saline (PBS) containing 1 mM dithiothreitol (DTT) by repeated passages through a 25G needle and then centrifuged at 500*g* for 10 minutes at 4°C to remove debris. Protein concentration of the supernatant was determined by the Bio-Rad DC Protein Assay (Bio-Rad Laboratories, Hercules, CA). The supernatant was mixed with SDS-PAGE sample buffer and boiled for 5 minutes. Forty μg of protein for brain and retina samples or 20 μg of protein for optic nerve sample were loaded onto 5–20% precast polyacrylamide gradient gels (Atto, Tokyo, Japan). The proteins were electrotransferred to a polyvinylidene difluoride (PVDF) membrane in Tris-glycine-methanol transfer buffer. The membrane was blocked for 1 hour at room temperature in buffer 1 (150 mM NaCl, and 100 mM Tris-HCl, pH 7.5) containing 2% blocking reagent (Roche Diagnostics, Penzberg, Germany) (buffer 2) and then incubated for 16 hours at 4°C with the anti-Wfs1 antibody (1:1,000) in blocking solution (buffer 2). The membrane was then rinsed with PBS three times and incubated for 1 hour at room temperature with peroxidase-conjugated affinipure $F(ab')_2$ fragment goat antirabbit IgG (H+L) (1:2,000) (Jackson ImmunoResearch Laboratories, West Grove, PA). Antigen-antibody complexes were visualized by enhanced chemiluminescence (ECL) system (GE Healthcare UK, Buckinghamshire, UK) and exposed onto Fuji medical x-ray films (RX-U) (Fujifilm, Tokyo, Japan).

To determine the specificity of anti-Wfs1 antibody we preabsorbed the antibody with GST-Wfs1N chimeric protein (antigen). The antigen (50 μg/mL) was incubated with the anti-Wfs1 antibody (1:1,000) for 3 hours at 4°C before incubation with the PVDF membrane, then the immunoblot was performed as described above. The GST-Wfs1N chimeric protein was newly generated. The service offered by Hokudo (Sapporo, Japan) was used to produce the protein. The protocols were the same as described above except for the strain of *E. coli*. For expression of the protein the B21(DE3)RIL strain was used instead of the JM109 strain.

TABLE 1. Primary Antibodies Used in This Study

Antibody	Manufacturer	Catalog No.	Lot No.	Antibody isotype	Clone	Dilution	Antigen	Specificity
Mouse Wfs1	This Study			Rabbit serum		1:5000-1:10000	Amino acids 1-179 representing N-terminus Wfs1 protein of mouse origin	A single band of ≈100 kDa in extracts from the mouse brain and optic nerve. ≈100 kDa and ≈70 kDa bands in extracts from the mouse retina. Antigen block of immunolabeling. Figs. 1 and 2D
Calbindin-D-28K	Sigma-Aldrich, St. Louis, MO	C9848	113K4867	Mouse IgG_1	Clone CB-955	1:500	Purified bovine kidney calbindin-D-28K	A single 28-kDa band.[1] Staining pattern identical to published data[2]
Goα	Chemicon, Temecula, CA	MAB3073	24040782	Mouse IgG_1	Clone 2A	1:250	Purified bovine brain Goα	A single protein band of 39-42 kDa.[1] Staining pattern identical to published data[2]
Choline Acetyltransferase	Chemicon	AB144P	24030848	Goat serum		1:100	Choline acetyltransferase from human placenta	Staining pattern identical to published data[3]
Tubulin, βIII isoform	Chemicon	MAB1637	25010305	Mouse IgG_1	Clone TU-20	1:50	A synthetic peptide corresponding to amino acids 443-450 (ESESQGPK) of human class III β-tubulin conjugated to keyhole limpet hemocyanin (KLH), a carrier for haptens	A single protein band of 50 kDa in extracts from the porcine brain[4]
Brn-3a	Santa Cruz Biotechnology, Santa Cruz, CA	sc-8429	L1106	Mouse IgG_{2b}	Clone 14A6	1:50	Amino acids 1-109 representing N-terminus Brn-3a protein of mouse origin	Staining pattern identical to published data[5]
Glutamine Synthetase	BD Biosciences Pharmingen, San Diego, CA	610517	01915	Mouse IgG_{2a}	Clone 6	1:500	Sheep glutamine synthetase (1-373: Full Length)	A single protein band of 45 kDa in extracts from the rat brain[6]
Glial Fibrillary Acidic Protein (GFAP)	Chemicon	AB5804	23080114	Rabbit serum		1:1000	Purified bovine GFAP	A single protein band of 51 kDa in extracts from the mouse brain[7]
GFAP	Chemicon	MAB360	25040157	Mouse IgG_1	Clone GA5	1:1000	Purified GFAP from porcine spinal cord	A single protein band of 51 kDa in extracts from a human glioma cell line.[8].Staining pattern (Fig. 8B) identical to that of the anti-GFAP rabbit serum (Fig. 6A)
Oligodendrocytes [RIP]	Chemicon	MAB1580	25040064	Mouse IgG_1	Clone NS-1	1:100000	Rat olfactory bulb	Staining pattern identical to published data[9]
Mouse CD11b (Mac-1 α chain)	BD Biosciences Pharmingen	550282	01651	Rat (DA) $IgG_{2b,\kappa}$	Clone M1/70	1:50	C57BL/10 mouse splenic T cells and concanavalin A-activated C57BL/10 splenocytes	Staining pattern identical to published data[10]

[1]Manufacturer's technical information; Gargini et al., 2007.
[2]Haverkamp and Wässle, 2000.
[3]Jeon et al., 1998; Haverkamp and Wässle, 2000; Kang et al., 2004.
[4]Manufacturer's technical information; Dráberová et al., 1998.
[5]Xiang et al., 1995.
[6]Manufacturer's technical information.
[7]Jalil et al., 2005.
[8]Manufacturer's technical information; Debus et al., 1983.
[9]Saari et al., 1997; Morcos and Chan-Ling, 2000.
[10]Retina: Dräger, 1983; Optic nerve: Reichert and Rotshenker, 1996; Neufeld, 1999.

In situ hybridization histochemistry

To synthesize a cRNA probe for in situ hybridization an 870-base fragment of the mouse *Wfs1* cDNA was amplified by reverse-transcriptase polymerase chain reaction (RT-PCR) and subcloned into the vector pCR-Blunt (Invitrogen, Carlsbad, CA). The primers used were No. 00276, 5′-CGG GAT CCA TGA ACT CAG GCA CCC CAC CT-3′, and No. 00277, 5′-GGA ATT CCA CCT TCT GGC GTA GTG GCA G-3′. The fragment encoded the 5′-end of the protein-coding region, including all of exon 2 and the first triplet of exon 3. Two independent clones containing the insert with a different orientation (pCR-clone 3 for sense, pCR-clone 9 for antisense) were used. A sense or an antisense cRNA probe was obtained by in vitro transcription with a DIG RNA labeling kit (SP6/T7; Roche Diagnostics).

In situ hybridization histochemistry was carried out as described previously (Fujinaga et al., 2004). Free-floating sections washed for 5 minutes in diethylpyrocarbonate-treated PBS (DEPC-PBS) were pretreated with 0.2 N HCl for 20 minutes, washed twice for 5 minutes in DEPC-PBS, and then acetylated in 0.1 M triethanolamine-HCl (pH 8.0) containing 0.25% acetic anhydride for 10 minutes. Before the hybridization step, sections were washed again twice for 5 minutes with DEPC-PBS. All pretreatments were performed at 4°C. Following the pretreatment, sections were preincubated in hybridization buffer (50% deionized-formamide; 10 mM Tris-HCl, pH 7.5; 1 mM EDTA, pH 8.0; 600 mM NaCl; 1 × Denhardt's solution; 10% dextran sulfate; 0.25% sodium dodecyl sulfate; and 200 μg/mL yeast tRNA) at 55°C for 1 hour and then hybridized with DIG-labeled anti-sense cRNA probes (0.5 μg/mL; denatured at 95°C for 5 minutes and cooled at 4°C for 5 minutes shortly before use) in the same buffer at 55°C for 16 hours. After hybridization, the sections were washed with 2 × SSC (300 mM NaCl, and 30 mM sodium citrate, pH 7.0) containing 50% formamide at 55°C for 1 hour, rinsed in wash buffer (500 mM NaCl, 10 mM Tris-HCl, pH 8.0, and 1 mM EDTA, pH 8.0) for 10 minutes, and then incubated with RNase A (20 μg/mL; Sigma-Aldrich, St. Louis, MO) in wash buffer at 37°C for 30 minutes. After being rinsed in wash buffer again for 10 minutes, they were soaked in 2 × SSC containing 50% formamide and 0.2 × SSC containing 50% formamide at 55°C for 30 minutes each. To perform the immunoreaction the sections were blocked in buffer 2 (buffer 1 [150 mM NaCl, and 100 mM Tris-HCl, pH 7.5] containing 2% blocking reagent) at 20°C for 1 hour and then incubated in buffer 2 containing alkaline phosphatase-conjugated sheep anti-DIG antibody (Roche Diagnostics) diluted 1:3,000 at 20°C for 16 hours. After two washes in buffer 1 for 10 minutes they were rinsed in buffer 3 (100 mM NaCl, 50 mM $MgCl_2$, 100 mM Tris-HCl, pH 9.5) for 5 minutes and incubated with NBT/BCIP substrate (1:50; Roche Diagnostics) in buffer 3 at 37°C for 2–4 hours to visualize the immunocomplex. The coloring reaction was stopped with buffer 4 (1 mM EDTA, and 10 mM Tris-HCl, pH 8.0), and the sections were washed in PBS, mounted on glass slides using a 0.6% gelatin solution, and air-dried. The slides were coverslipped with VectaMount mounting medium (Vector Laboratories, Burlingame, CA). As a control, a sense cRNA probe was used instead of the antisense cRNA probe. Signals detected by the antisense *Wfs1* cRNA probe were categorized as positive if they were stronger than those detected by the sense probe in an adjacent section (control section).

Immunohistochemistry

Single immunoperoxidase staining. Sections of the retina, the optic nerve, and the brain were processed by the immunoperoxidase method as previously described (Sheng et al., 2004). Free-floating sections were bleached for 1 hour with 50% methanol and 1.5% hydrogen peroxide diluted with Milli-Q water at 4°C, and they were washed three times each for 15 minutes in PBS containing 0.3% Triton X-100 (PBST). The sections were preincubated for 2 hours with 10% normal goat serum (NGS) in 0.1 M PB containing 0.3% Triton X-100 (10% NGS blocking solution) at 4°C. The sections were incubated for 3 days with the anti-Wfs1 antibody diluted 1:10,000 in a 10% NGS blocking solution at 4°C. After the primary immunoreaction, primary antibody was washed out with PBST. Then the sections were incubated for 3 hours at 4°C with biotinylated antirabbit goat IgG (Dako Cytomation, Glostrup, Denmark; 1:500) in PBS containing 5% NGS. After the secondary immunoreaction the sections were washed three times each for 10 minutes in PBS and incubated for 3 hours at 4°C with a mixture of rabbit peroxidase anti-peroxidase (PAP; Dako Cytomation, 1:500) and peroxidase-conjugated streptavidin (Dako Cytomation, 1:500) in PBS containing 1% NGS (enhanced HRP-labeling reaction). Then they were washed three times each for 15 minutes in 0.05 M Tris-HCl buffer (pH 7.6) and subjected to a dark-violet-black coloring reaction with 0.02% 3,3′-diaminobenzidine tetrahydrochloride (DAB; Wako Pure Chemical Industries, Osaka, Japan) and 0.6% nickel ammonium sulfate hexahydrate in 0.05 M Tris-HCl buffer (pH 7.6) containing 0.0006% hydrogen peroxide for 10–15 minutes at 4°C. After three washes in PBS the sections were mounted onto glass slides in a 0.6% gelatin solution. After being air-dried they were dehydrated with a graded series of ethanol solutions, immersed in xylene, and embedded in NEW M · X mountant (Matsunami, Osaka, Japan).

To determine the specificity of the anti-Wfs1 antibody in sections the GST-Wfs1N chimeric protein (5 μg/mL) was incubated with the anti-Wfs1 antibody (1:10,000) for 6 hours at 4°C before incubation with sections of the retina, the optic nerve, and of the brain, and then immunohistochemistry was performed as described above. To verify the nonspecific immunoreaction by the secondary antibody (biotinylated antirabbit goat IgG), normal rabbit immunoglobulin (Dako Cytomation) was used instead of the primary antibody (anti-Wfs1). For the cytoarchitectonic analysis, adjacent series of the brain sections were subjected to Nissl staining by using cresyl violet (acetate) (Merck, Darmstadt, Germany).

Single and double immunofluorescent staining. To identify cell types expressing Wfs1, we performed double immunohistochemistry in retinal and optic nerve tissue. The monoclonal and goat polyclonal antibodies listed in Table 1 were used for additional primary antibodies. In experiments using the mouse monoclonal antibodies, free-floating sections were preincubated for 2 hours in a 10% NGS blocking solution at 4°C, then immunoreacted for 4 days with a mixture of the anti-Wfs1 antibody (1:5,000) and each of the monoclonal antibodies in a 10% NGS blocking solution at 4°C. After three rinses for 10 minutes in PBST the sections were incubated with a mixture of two secondary antibodies in PBS containing 5% NGS and 0.3% Triton X-100 for 24 hours at 4°C. The two secondary antibodies used were Alexa Fluor 488 conjugated with the $F(ab')_2$ fragment of goat antirabbit IgG (H+L) (1:200; Molecular Probes) and Alexa Fluor 594 conjugated to the $F(ab')_2$ fragment of goat antimouse IgG (H+L) (1:200; Molecular Probes). The sections were washed three times for 10 minutes in PBS and mounted onto glass slides in a 0.6% gelatin solution. After being air-dried the sections were subjected to nuclear staining by using a bisBenzimide (Hoechst 33258, Sigma-Aldrich, 0.1 mg/mL) solution, and coverslipped with Vectashield mounting medium (Vector Laboratories). For staining using the rat monoclonal antibody, Alexa Fluor 488 conjugated to goat antirabbit IgG (H+L), highly cross-absorbed (1:200; Molecular Probes) and Alexa Fluor 568 conjugated to goat antirat IgG (H+L) (1:200; Molecular Probes) were used as second-

ary antibodies. For staining using the goat polyclonal antibody, normal donkey serum was used instead of NGS. As for secondary antibodies, Alexa Fluor 488 conjugated to donkey antirabbit IgG (H+L) (1:200; Molecular Probes) and Alexa Fluor 594 conjugated to donkey antigoat IgG (H+L) (1:200; Molecular Probes) were used.

In double immunohistochemistry for detecting GFAP and GS simultaneously in the optic nerve, the rabbit polyclonal anti-GFAP antibody (1:1,000) and the mouse monoclonal anti-GS antibody (1:500) were used as primary antibody. Other procedures were the same as those for double immunohistochemistry by using the anti-Wfs1 and each of the mouse monoclonal antibodies. To eliminate the possibility of any crossreaction between secondary antibodies and primary antibodies from the wrong species, one of the two primary antibodies was removed. In these control experiments no crossreactivity was observed (data not shown).

Single immunofluorescent staining was applied to Wfs1/tracer double labeling. The anti-Wfs1 antibody (1:5,000) alone was used for primary antibody, and Alexa Fluor 488 conjugated with the $F(ab')_2$ fragment of goat antirabbit IgG (H+L) (1:200; Molecular Probes) alone for secondary antibody. Other procedures were the same as those for double immunohistochemistry by using the anti-Wfs1 and each of the mouse monoclonal antibodies. In Fluorescent Latex Microspheres injection cases a coverslip was made by using Fluoromount-G (SouthernBiothech, Birmingham, AL) instead of the Vectashield mounting medium (Vector Laboratories) in order to prevent Fluorescent Latex Microspheres from fading (manufacturer's technical information by Lumafluor).

To determine Wfs1-specific immunoreactivity in Wfs1/Goα and Wfs1/FLM double-labeling studies, the anti-Wfs1 antibody (1:5,000) was preabsorbed with the antigen (50 μg/mL) as described in the "Single immunoperoxidase staining" section.

Photomicrographs and terminology

Brightfield photomicrographs were taken using a DS-5Mc color digital camera (Nikon, Tokyo, Japan) equipped with an Eclipse 80i photomicroscope (Nikon). Fluorescence photomicrographs were taken with a FV500 confocal laser scanning microscope (Olympus, Tokyo, Japan) at the Center for Chronic Viral Diseases, Kagoshima University Graduate School of Medical and Dental Sciences, or a LSM510 (Carl Zeiss, Jena, Germany) at the Institute for Biomedical Research and Education in Yamaguchi University Science Research Center. Images were transferred to Adobe Photoshop 6 (Adobe Systems, San Jose, CA) and brightness, contrast, and picture sharpness were adjusted. No other adjustment was made.

The nomenclature used for the different regions of the brain follows that of Paxinos and Franklin (2001).

RESULTS

Immunoblot analysis of Wfs1 protein expression

To determine organ-specific Wfs1 protein expression in the brain, retina, and optic nerve, and to characterize the specificity of the anti-Wfs1 antibody, we performed immunoblot analysis. The anti-Wfs1 antibody detected Wfs1 protein bands of ≈100 kDa in extracts from the brain, retina, and optic nerve. In addition, a Wfs1-immunoreactive band of ≈70 kDa in extracts from the retina was observed (Fig. 1, anti-Wfs1). These protein bands were not seen when extracts from the brain, retina, and optic nerve were incubated with the anti-Wfs1 antibody preabsorbed by incubation with the GST-Wfs1N chimeric protein (antigen) (Fig. 1, Absorbed).

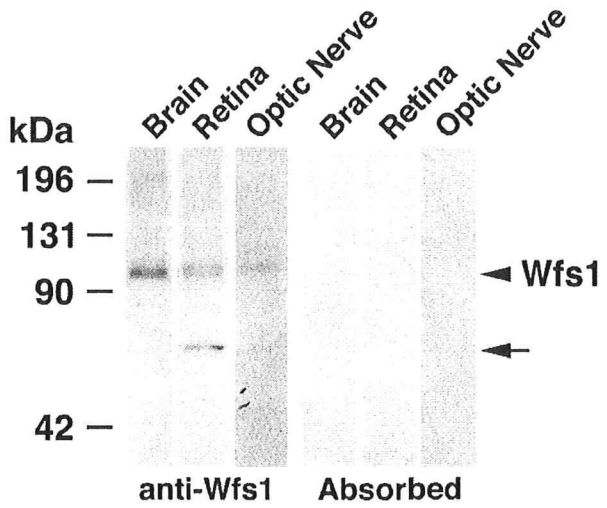

Fig. 1. Wfs1 protein immunoreactivity in the normal mouse brain, retina, and optic nerve. Immunoblot of extracts from the normal mouse brain, retina, and optic nerve probed with rabbit antimouse Wfs1 N-terminus antibody (anti-Wfs1), and with the antibody preabsorbed by incubation with GST-Wfs1 N-terminus chimeric protein (Absorbed). The arrowhead indicates Wfs1 protein bands of ≈100 kDa in extracts from the brain, retina, and optic nerve (anti-Wfs1). The arrow shows a Wfs1 immunoreactive band of ≈70 kDa in extracts from the retina (anti-Wfs1). These bands are not seen in the antibody-absorption experiment (Absorbed). Positions of size markers are indicated on the left.

Wfs1 mRNA expression in the normal mouse retina

To determine cell-specific *Wfs1* expression in retinal cells we performed RNA in situ hybridization on normal mouse retinal sections by using a mouse *Wfs1* antisense-riboprobe. The most intense *Wfs1* mRNA signals were observed in cell bodies of the ganglion cell layer (GCL; Fig. 2A). Moderate signals were distributed in the inner and outer rows of the inner nuclear layer (INL), and in the inner segment of photoreceptors (PR). The moderate signals in the outer row showed a dash-shaped appearance and were located along the boundary between the INL and outer plexiform layer (OPL). Weak signals were seen in the intermediate row of the INL and outer nuclear layer (ONL; Fig. 2A). Few detectable signals were found in control experiments with a mouse *Wfs1* cRNA sense probe. In these experiments there was a tendency for reaction deposits to be randomly scattered over the entire retina, including the inner plexiform layer (IPL; Fig. 2B).

Wfs1 protein expression in the normal mouse retina

To examine cell-specific protein localization, retinal sections were immunostained by using the anti-Wfs1 anti-

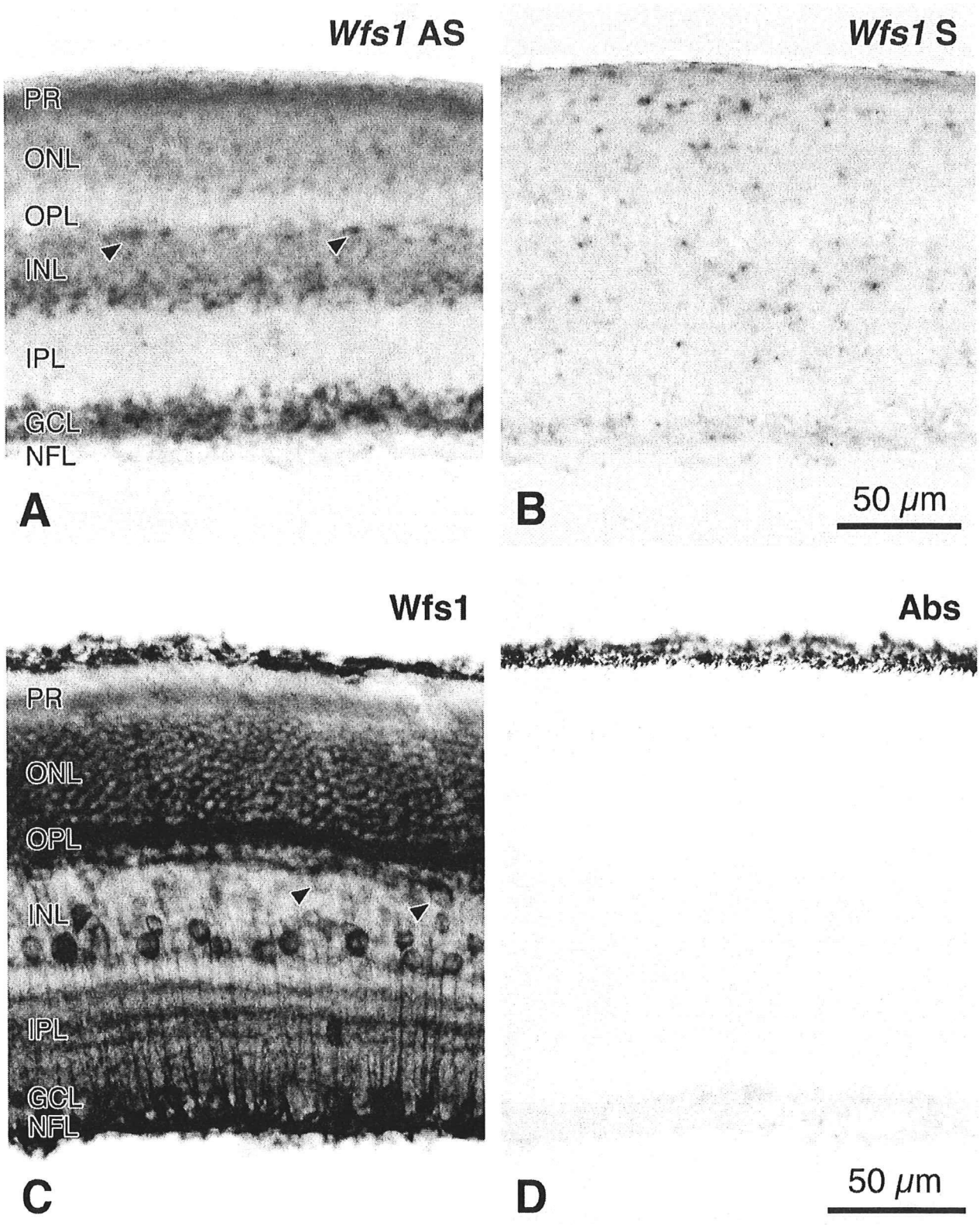

Fig. 2. *Wfs1* mRNA signals and protein immunoreactivity in the normal mouse retina. **A,B:** Mouse *Wfs1* mRNA signals in two adjacent sections of the retina hybridized with antisense cRNA probes of the mouse *Wfs1* 5′-terminus (*Wfs1* AS; A), and with sense cRNA probes (*Wfs1* S; B). Arrowheads indicate moderate *Wfs1* mRNA signals in the outer row of the inner nuclear layer (INL). **C,D:** Mouse Wfs1 protein immunoreactivity in two sections of the retina immunostained with rabbit antimouse Wfs1 N-terminus antibody (Wfs1; C), and with the antibody preabsorbed by incubation with GST-Wfs1 N-terminus chimeric protein (antigen) (Abs; D). Arrowheads indicate Wfs1-immunoreactive neurons, of which cell bodies are weakly labeled and processes are moderately labeled, in the outer row of the INL. Note that a substantial number of *Wfs1* mRNA signals and a considerable amount of protein immunoreactivity are seen not only in the ganglion cell layer but also in the inner and the outer nuclear layers of the normal mouse retina. PR, photoreceptor; ONL, outer nuclear layer; OPL, outer plexiform layer; INL, inner nuclear layer; IPL, inner plexiform layer; GCL, ganglion cell layer; NFL, optic nerve fiber layer. Scale bars = 50 μm in B,D apply to A,C, respectively.

body. The most intense immunoreactivity was observed in the OPL, the inner row of the INL, the GCL, and in the optic nerve fiber layer (NFL). Moderate immunoreactivity was found in the inner segment of PR, the ONL, and in the outer row of the INL. In the outer row of the INL, Wfs1-immunoreactive cell bodies were seen with their processes extending along the intense immunoreactivity in the OPL (arrowheads in Fig. 2C). Weakly Wfs1-immunoreactive cell bodies were seen in the middle row of the INL. In the IPL three labeled strata were observed and the immunoreactivity in the intermediate stratum was stronger than that in the other two strata. Radially extending Wfs1-immunoreactive fibers were clearly seen from the INL to the NFL with these fibers terminating at the inner limiting membrane (Fig. 2C). When a normal rabbit immunoglobulin was used instead of the anti-Wfs1 antibody, as a control for Wfs1 immunohistochemistry, no clear immunoreactivity by the secondary antibody was seen in cytoplasms of the normal mouse retina (data not shown). When the antibody preabsorbed by incubation with the GST-Wfs1N chimeric protein (antigen), no clearly immunoreactive cytoplasm was observed (Fig. 2D).

To confirm which cell types express Wfs1, retinal sections or whole-mount retinae were double-immunostained with the anti-Wfs1 antibody and with each of the antibodies against several retinal marker proteins. In the outer row of the INL, Wfs1 immunoreactivity was observed in horizontal cells, which were immunolabeled with antibodies against calbindin-D-28K (a horizontal cell marker). In these cells the intensity of Wfs1 immunoreactivity was weak-to-moderate and the immunoreactivity was seen in both cell bodies and processes (Fig. 3A–C). In the outer and intermediate rows of the INL, faint Wfs1 immunoreactivity was detected in putative ON-cone, and rod bipolar cells, which were immunolabeled with antibodies against G-protein Goα (a bipolar cell marker; Fig. 3D–F). In control (preabsorption) experiments, Wfs1 immunoreactivity was hardly seen in Goα-immunoreactive bipolar cells (Fig. 3G–I; compare 3D with 3G). In the inner row of the INL, strong Wfs1 immunoreactivity was observed in nondisplaced amacrine cells, which were immunolabeled with antibodies against ChAT (a cholinergic amacrine cell marker; Fig. 3J–L) or against calbindin-D-28K (an amacrine cell marker; Fig. 3M–O). In the IPL the three Wfs1-immunoreactive strata were overlapped with three calbindin-D-28K-immunoreactive strata (Fig. 3M–O). Out of these strata the outer and inner ones were overlaid with two cholinergic strata (Fig. 3J–L).

In the GCL, strong Wfs1 immunoreactivity was observed in cholinergic displaced amacrine cells, which were immunolabeled with antibodies against ChAT (a cholinergic amacrine cell marker; Fig. 4A–F). In addition, Wfs1-immunoreactive but noncholinergic cells were distributed in this layer (Fig. 4A–C). To examine whether these cells are RGCs, we performed Wfs1/tracer double labeling and Wfs1/retinal ganglion cell-specific-marker double immunofluorescent staining. Wfs1 immunoreactivity was detected in RGCs that were retrogradely labeled in vivo with Fluorescent Latex Microspheres (Fig. 4G–I) or with Fluoro-Ruby (Fig. 5A–C). Additionally, Wfs1 immunoreactivity was also detected in RGCs that were immunolabeled with antibodies against tubulin, βIII isoform (Fig. 4M–O), or Brn-3a POU-domain transcription factor (Fig. 4P–R). To verify whether Wfs1 immunoreactivity is positive in RGCs, we performed control (preabsorption) experiments. In these experiments, Wfs1 immunoreactivity was hardly seen in Fluorescent Latex Microspheres-labeled RGCs (Fig. 4J–L; compare 4G with 4J). There is a tendency that Wfs1 immunoreactivity in cholinergic displaced amacrine cells is stronger than that in RGCs. Thus, immunoreactivity for Wfs1 was observed in all neuron types: photoreceptors, horizontal cells, bipolar cells, nondisplaced and displaced amacrine cells, and RGCs (Figs. 3, 4, 5A–C).

In glial cells, immunoreactivity for Wfs1 was observed solely in Müller cells, which were exclusively immunolabeled with antibodies against GS. In Müller cells, Wfs1 immunoreactivity was strong in the endfeet adjacent to the inner limiting membrane, moderate in internal radial processes, but weak in their cell bodies localized to the intermediate row of the INL (Fig. 5D–F). Wfs1 immunoreactivity was not seen in GFAP-immunoreactive astrocytes, or mouse CD11b-immunoreactive microglia (Table 2).

Optic nerve

Because a definition of the optic nerve subdivision is necessary for the description and interpretation of the experimental results, we will briefly describe our criteria for determining the border of each part of the optic nerve.

Fig. 3. Cellular localization of Wfs1 in the inner nuclear layer of the normal mouse retina. **A–C:** Wfs1 immunoreactivity in horizontal cells. A retinal section was double-immunostained for Wfs1 (Wfs1; A; Alexa Fluor 488 label; green) and for a horizontal cell marker (calbindin-D-28K, CalD28K; B; Alexa Fluor 594 label; red). Cell nuclei are labeled in blue with bisBenzimide (Hoechst 33258; B,C). C is an overlaid image. Arrows indicate a horizontal cell immunoreactive for Wfs1. **D–F:** Wfs1 immunoreactivity in bipolar cells. A retinal section was double-immunostained for Wfs1 (Wfs1; D; Alexa Fluor 488 label; green) and for a bipolar cell marker (G-protein Goα, Goα; E; Alexa Fluor 594 label; red). Cell nuclei are labeled in blue with bisBenzimide (Hoechst 33258; E,F). F is an overlaid image. Arrows and arrowheads show a putative ON-cone bipolar and a rod bipolar cells that are immunoreactive for Wfs1, respectively. **G–I:** A control experiment of Wfs1 immunoreactivity in bipolar cells. An adjacent retinal section of D–F was double-immunostained for Wfs1 after a preabsorption procedure (Wfs1 Abs; G; Alexa Fluor 488 label; green) and for Goα (H; Alexa Fluor 594 label; red). Cell nuclei are labeled in blue with bisBenzimide (Hoechst 33258; H,I). I is an overlaid image. Arrows and arrowheads show a putative ON-cone bipolar and a rod bipolar cell that are not immunoreactive for Wfs1, respectively. **J–O:** Wfs1 immunoreactivity in nondisplaced amacrine cells. A retinal section was double-immunostained for Wfs1 (Wfs1; J; Alexa Fluor 488 label; green) and for a nondisplaced amacrine cell marker (choline acetyltransferase, ChAT; K; Alexa Fluor 594 label; red). Another section was double-immunostained for Wfs1 (Wfs1; M; Alexa Fluor 488 label; green) and for another nondisplaced amacrine cell marker (calbindin-D-28K, CalD28K; N; Alexa Fluor 594 label; red). Cell nuclei are labeled in blue with bisBenzimide (Hoechst 33258; N,O). L and O are overlaid images. Arrowheads indicate nondisplaced amacrine cells immunoreactive for Wfs1. These fluorescence photomicrographs were taken with an FV500 confocal microscope (Olympus). Note that Wfs1 immunoreactivity is observed in photoreceptors, horizontal cells, bipolar cells, and in nondisplaced amacrine cells. ONL, outer nuclear layer; OPL, outer plexiform layer; INL, inner nuclear layer; IPL, inner plexiform layer; GCL, ganglion cell layer. Scale bar = 20 μm in O applies to A–N.

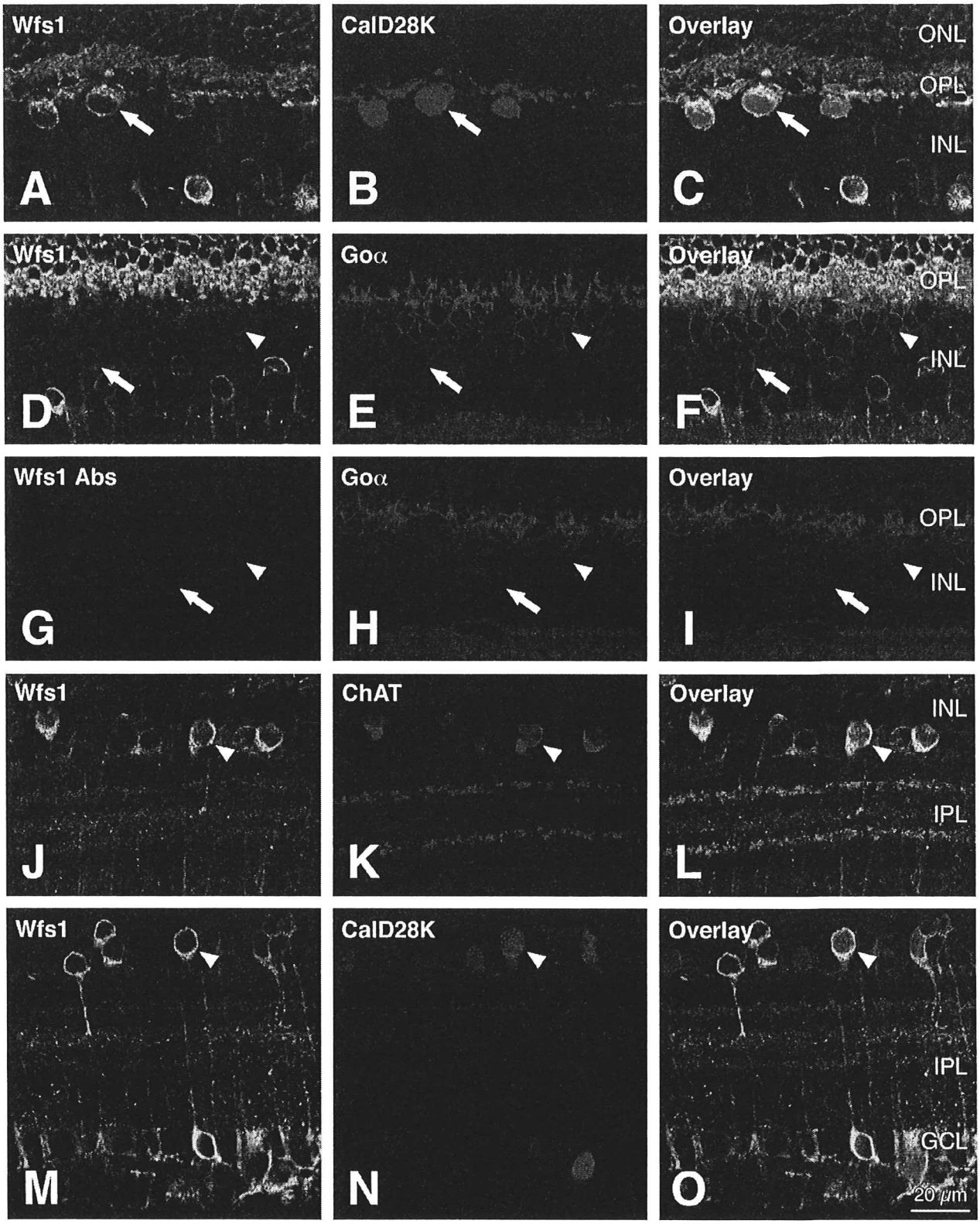
Wfs1
CalD28K
Overlay
ONL
OPL
INL
A
B
C
Wfs1
Goα
Overlay
OPL
INL
D
E
F
Wfs1 Abs
Goα
Overlay
OPL
INL
G
H
I
Wfs1
ChAT
Overlay
INL
IPL
J
K
L
Wfs1
CalD28K
Overlay
IPL
GCL
M
N
O
20 μm

Figure 3

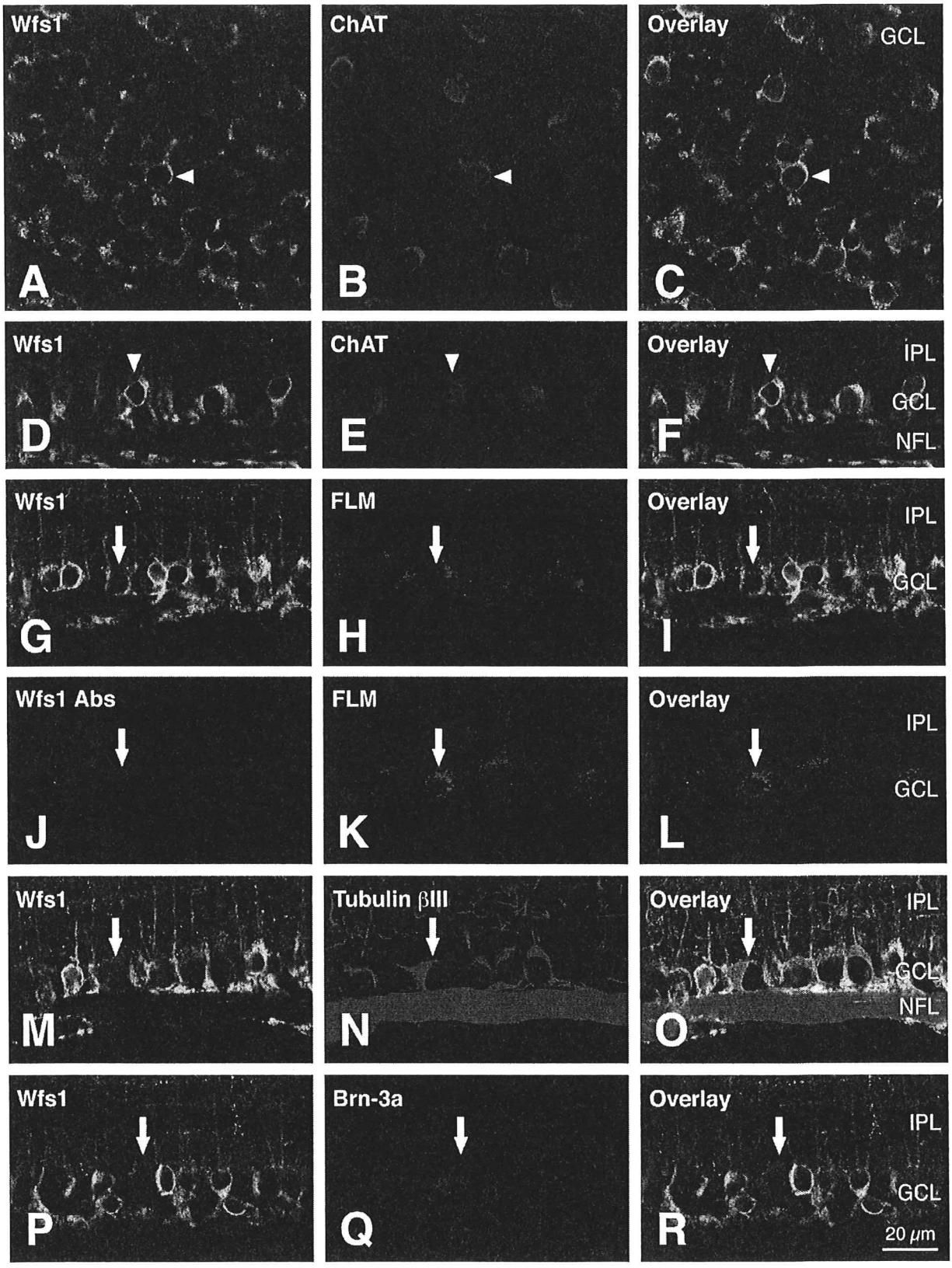
Wfs1
ChAT
Overlay
GCL
A
B
C
Wfs1
ChAT
Overlay
IPL
GCL
NFL
D
E
F
Wfs1
FLM
Overlay
IPL
GCL
G
H
I
Wfs1 Abs
FLM
Overlay
IPL
GCL
J
K
L
Wfs1
Tubulin βIII
Overlay
IPL
GCL
NFL
M
N
O
Wfs1
Brn-3a
Overlay
IPL
GCL
20 μm
P
Q
R

Figure 4

In the orbit the mouse optic nerve was divided into three parts: intraretinal (i), astrocytic filament dense (afd), and astrocytic filament sparse (afs). This classification was defined by the position of the sensory retina and by the distribution of astrocytic filaments. The border between the i and afd parts was set at the boundary between the sensory retina and the retinal pigment epithelium. Astrocytic filaments were seen to be elongated transversely at the border (Fig. 6A,C), while those in the i part were observed to be extended longitudinally. In the afd part a very high concentration of astrocytic filaments was seen. A majority of astrocytic filaments in the afs part were long and extended perpendicular to the optic nerve axis, while a minority were seen to be short and expanded parallel to the axis. The border between the afd and afs parts was defined by the distal (anterior) limit of longer transverse filaments in the afs part (Fig. 6A,C). The length of the afd part was around 200 μm. The area containing GS-immunoreactive cells in the mouse optic nerve corresponded to the afs part (Fig. 6).

Wfs1 mRNA expression in the normal mouse optic nerve

Next, to determine whether *Wfs1* mRNA is expressed in the optic nerve we performed RNA in situ hybridization on longitudinal sections of the normal mouse optic nerve by using a mouse *Wfs1* antisense-riboprobe. Weak-to-moderate *Wfs1* mRNA signals were observed in the afd and afs parts. In the afd part, *Wfs1* mRNA-hybridized cells were densely concentrated, while in the afs part they were sparsely distributed. Weak *Wfs1* mRNA signals were detected in the i part (Fig. 7A). In control experiments by using a mouse *Wfs1* cRNA sense probe few mRNA signals were observed (Fig. 7B).

TABLE 2. Distribution of Wfs1 Immunoreactivity in the Normal Mouse Retina

Retinal Cells	
Photoreceptor	+
Outer plexiform layer	+
Horizontal cells	+
Bipolar cells	+
Amacrine cells	+
Inner plexiform layer	+
Ganglion cells	+
Displaced amacrine cells	+
Müller cells	+
Astrocytes	–
Microglia	–

+, present; –, not present.

Wfs1 protein expression in the normal mouse optic nerve

We next examined cell-specific Wfs1 protein localization in the optic nerve. Weak-to-moderate Wfs1 immunoreactivity was clearly seen in the afd and afs parts (Fig. 7C,E,F). Wfs1-immunoreactive cells were aligned along optic nerve fiber bundles, and more tightly distributed in the afd than afs part. Background Wfs1 immunoreactivity on optic nerve fiber bundles was greater in the afd than afs part (Fig. 7C,E,F). Weak Wfs1 immunoreactivity was detected in the i part (Fig. 7C). When a normal rabbit immunoglobulin was used instead of the anti-Wfs1 antibody, no immunoreactivity was seen in the optic nerve (data not shown). When the antibody preabsorbed by incubation with the GST-Wfs1N chimeric protein (antigen), immunoreactivity was not observed (Fig. 7D).

To confirm which glial cell types express Wfs1, other longitudinal sections were double-immunostained with the anti-Wfs1 antibody, and with antibodies against GFAP (an astrocyte marker), oligodendrocytes [RIP] (an oligodendrocyte marker), GS (a glial cell marker), or mouse CD11b (a marker for microglia). Wfs1 immunoreactivity was observed solely in astrocytes (Fig. 8A–I). No Wfs1 immunoreactivity was found in oligodendrocytes (Fig. 8J–O), GS-immunoreactive glial cells (Fig. 8P–R), or in microglia (data not shown; Table 3).

Wfs1 mRNA expression in the normal mouse vision-related brain structures

We examined whether *Wfs1* mRNA was expressed in the optic chiasm, the optic tract, the retino-recipient nuclei, and in the visual cortex (vision-related brain structures). Moderate *Wfs1* mRNA signals were observed in layer II of the primary and secondary visual cortical areas. In layer II, moderate signals were distributed along the boundary between layers I and II, and weak signals were seen deeper down (Fig. 9A,C). In the retino-recipient nuclei, *Wfs1* mRNA signals were weak in the suprachiasmatic nucleus (SCN) and in the SC. In the SC, *Wfs1* mRNA-hybridized cells were dispersed in the zonal, superficial gray, and intermediate gray layers (Fig. 9D,F). Extremely weak or no *Wfs1* mRNA signals were seen in the optic chiasm, the optic tract, the LGN, the pretectum, and in the medial terminal nucleus (data not shown). In control experiments by using a mouse *Wfs1* cRNA sense probe, few mRNA signals were observed (data not shown).

Fig. 4. Cellular localization of Wfs1 in the ganglion cell layer of the normal mouse retina. **A–F:** Wfs1 immunoreactivity in displaced amacrine cells. A whole-mount retina (A–C) and a vertical retinal section (D–F) were double-immunostained for Wfs1 (Wfs1; A,D; Alexa Fluor 488 label; green) and for a displaced amacrine cell marker (choline acetyltransferase, ChAT; B,E; Alexa Fluor 594 label; red). Cell nuclei are labeled in blue with bisBenzimide (Hoechst 33258; B,C,E,F). C and F are overlaid images. Arrowheads indicate displaced amacrine cells immunoreactive for Wfs1. **G–I:** Wfs1 immunoreactivity in retinal ganglion cells (RGCs). Panels show a retinal section in which Wfs1 (G; Alexa Fluor 488 label; green) and Fluorescent Latex Microspheres (FLM; H; rhodamine label; red) double labeling was made. Cell nuclei are labeled in blue with bisBenzimide (Hoechst 33258; H,I). I is an overlaid image. Arrows indicate a retinal ganglion cell immunoreactive for Wfs1. **J–L:** A control experiment of Wfs1 immunoreactivity in RGCs. Wfs1 Abs; (J; Alexa Fluor 488 label; green) and FLM (K; rhodamine label; red) double labeling was performed in an adjacent retinal section of G–I after a preabsorption of the anti-Wfs1 antibody with the antigen. Cell nuclei are labeled in blue with bisBenzimide (Hoechst 33258; K,L). L is an overlaid image. Arrows indicate a retinal ganglion cell not immunoreactive for Wfs1. **M–R:** Wfs1 immunoreactivity in RGCs analyzed by double immunohistochemistry. A retinal section was double-immunostained for Wfs1 (Wfs1; M; Alexa Fluor 488 label; green) and for a ganglion cell marker (tubulin, βIII isoform, Tubulin βIII; N; Alexa Fluor 594 label; red). Another section was double-immunostained for Wfs1 (Wfs1; P; Alexa Fluor 488 label; green) and for another ganglion cell marker (Brn-3a POU-domain transcription factor, Brn-3a; Q; Alexa Fluor 594 label; red). Cell nuclei are labeled in blue with bisBenzimide (Hoechst 33258; N,O,Q,R). O and R are overlaid images. Arrows indicate RGCs immunoreactive for Wfs1. These fluorescence photomicrographs were taken with a FV500 confocal microscope (Olympus). Note that Wfs1 immunoreactivity is observed in both displaced amacrine cells and RGCs. IPL, inner plexiform layer; GCL, ganglion cell layer; NFL, optic nerve fiber layer. Scale bar = 20 μm in R applies to A–Q.

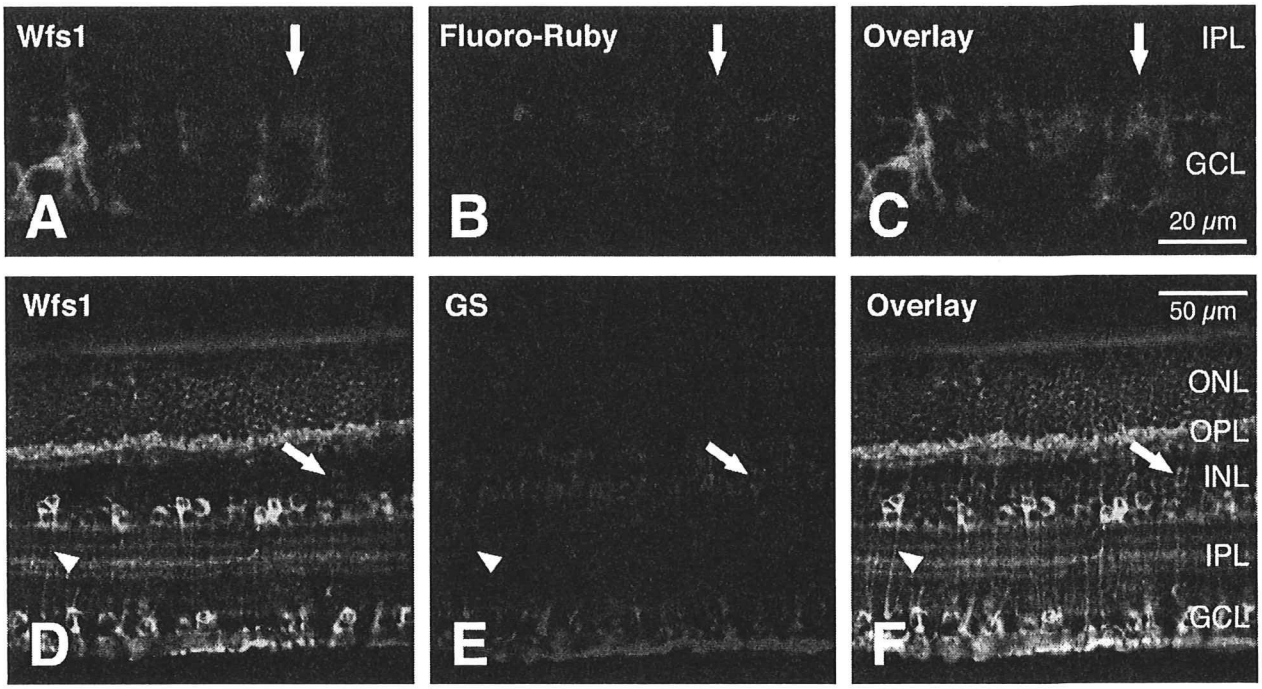

Fig. 5. Wfs1 immunoreactivity in retinal ganglion cells **(A–C)** and in Müller cells **(D–F)** of the normal mouse retina. A–C: Wfs1 (A; Alexa Fluor 488 label; green) and Fluoro-Ruby (B; tetramethylrhodamine label; red) double labeling. C is an overlaid image. Arrows indicate a retinal ganglion cell immunoreactive for Wfs1. D–F: Double immunostaining for Wfs1 (Wfs1; D; Alexa Fluor 488 label; green) and for a Müller cell marker (glutamine synthetase, GS; E; Alexa Fluor 594 label; red). F is an overlaid image. Arrows, and arrowheads show a cell body, and an inner process of Müller cells immunoreactive for Wfs1, respectively. Note that Wfs1 immunoreactivity is observed in Müller cells as well as in neurons of the retina. These fluorescence photomicrographs were taken with a LSM 510 confocal microscope (Carl Zeiss). ONL, outer nuclear layer; OPL, outer plexiform layer; INL, inner nuclear layer; IPL, inner plexiform layer; GCL, ganglion cell layer. Scale bars = 20 μm in C applies to A,B; 50 μm in F applies to D,E.

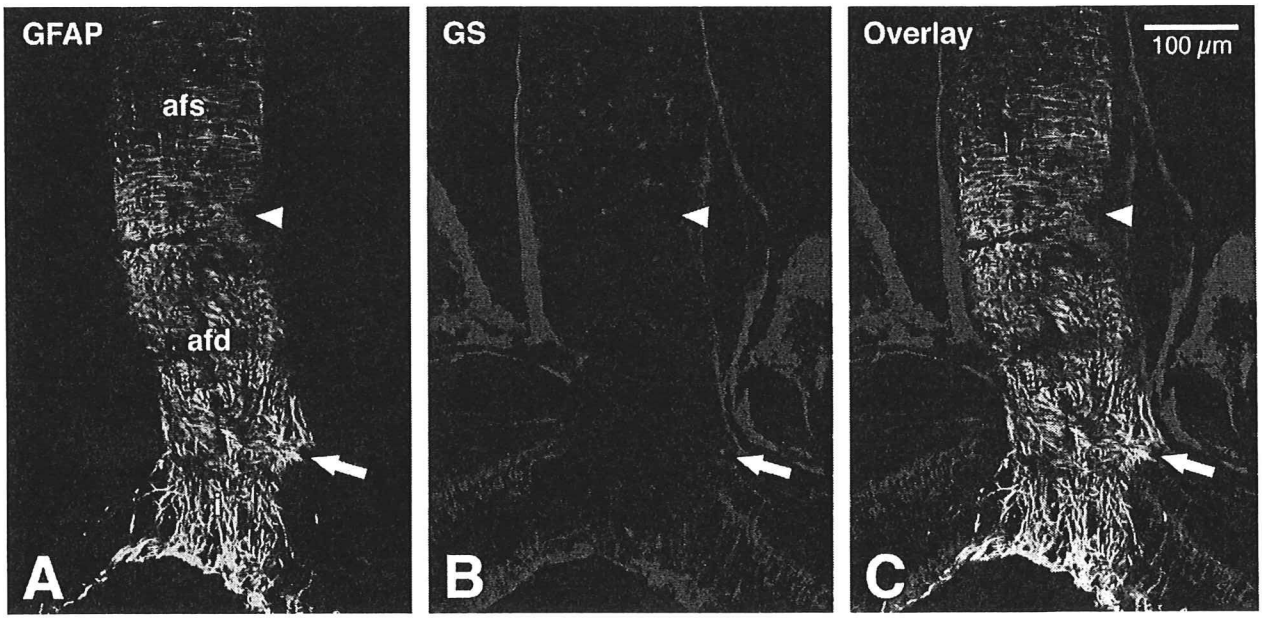

Fig. 6. Distribution of glial cells in the normal mouse optic nerve. Panels show double immunostaining for two glial cell markers, glial fibrillary acidic protein (GFAP; **A**; Alexa Fluor 488 label; green), and glutamine synthetase (GS; **B**; Alexa Fluor 594 label; red). **C:** An overlaid image. The mouse optic nerve is divided into three parts: intraretinal (i), astrocytic filament dense (afd), and astrocytic filament sparse (afs). Arrows, and arrowheads indicate the border between i and afd, and the boundary between afd and afs, respectively. These fluorescence photomicrographs were taken with a FV500 confocal microscope (Olympus). Note that the area containing GS-immunoreactive cells in the mouse optic nerve corresponds to the afs part. Scale bar = 100 μm in C applies to A,B.

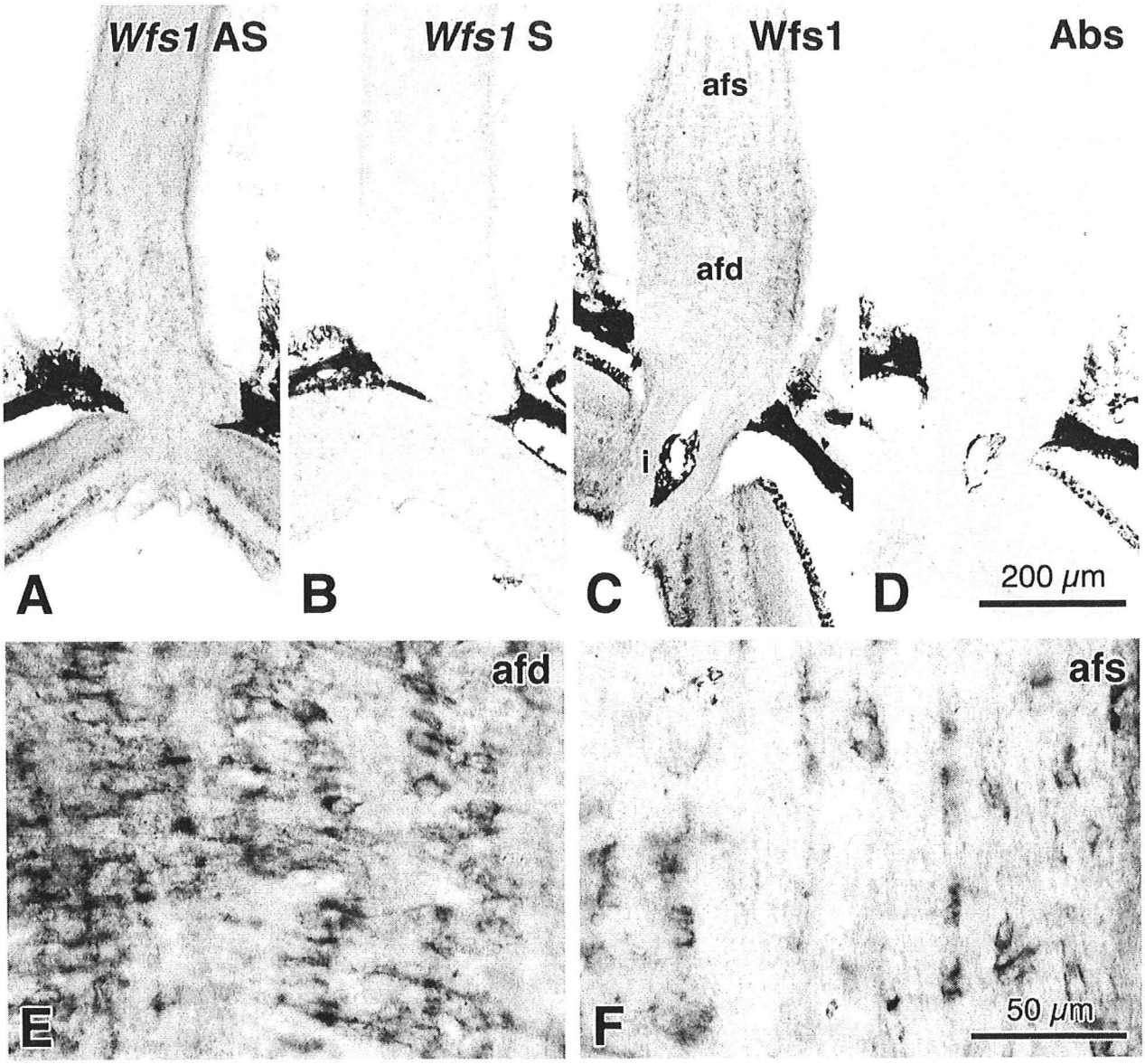

Fig. 7. *Wfs1* mRNA signals and protein immunoreactivity in the normal mouse optic nerve. **A,B:** Mouse *Wfs1* mRNA signals in two adjacent sections of the optic nerve hybridized with antisense cRNA probes of the mouse *Wfs1* 5′-terminus (*Wfs1* AS; A), and with sense cRNA probes (*Wfs1* S; B). **C,D:** Mouse Wfs1 protein immunoreactivity in two adjacent sections of the optic nerve immunostained with rabbit antimouse Wfs1 N-terminus antibody (Wfs1; C), and with the antibody preabsorbed by incubation with GST-Wfs1 N-terminus chimeric protein (antigen) (Abs; D). **E,F:** Higher magnification photomicrographs of mouse Wfs1 immunoreactivity in another adjacent section of C. E,F show Wfs1-immunoreactive cells in the astrocytic filament dense (afd) part, and those in the astrocytic filament sparse (afs) part, respectively. Note that both *Wfs1* mRNA signals and Wfs1 protein immunoreactivity are present in the mouse optic nerve. Scale bars = 200 μm in D applies to A–C; 50 μm in F applies to E.

Wfs1 protein expression in the normal mouse vision-related brain structures

We next examined whether Wfs1 protein was expressed in the vision-related brain structures. Wfs1 immunoreactivity was found in the visual cortex, the SCN, and in the SC (Figs. 9B,E, 10A). In the visual cortex, moderately Wfs1-immunoreactive neurons were distributed in layer II of the primary and secondary visual cortical areas. The more strongly immunoreactive neurons were distributed in the more superficial part of the layer. In addition, Wfs1-immunoreactive punctations were observed in layer V (Fig. 9B,C). In the SCN, moderately Wfs1-immunoreactive neurons were seen in the dorsomedial part (Fig. 10A). In the SC, moderately immunoreactive cells were distributed in the zonal, superficial gray, and intermediate gray layers (Fig.

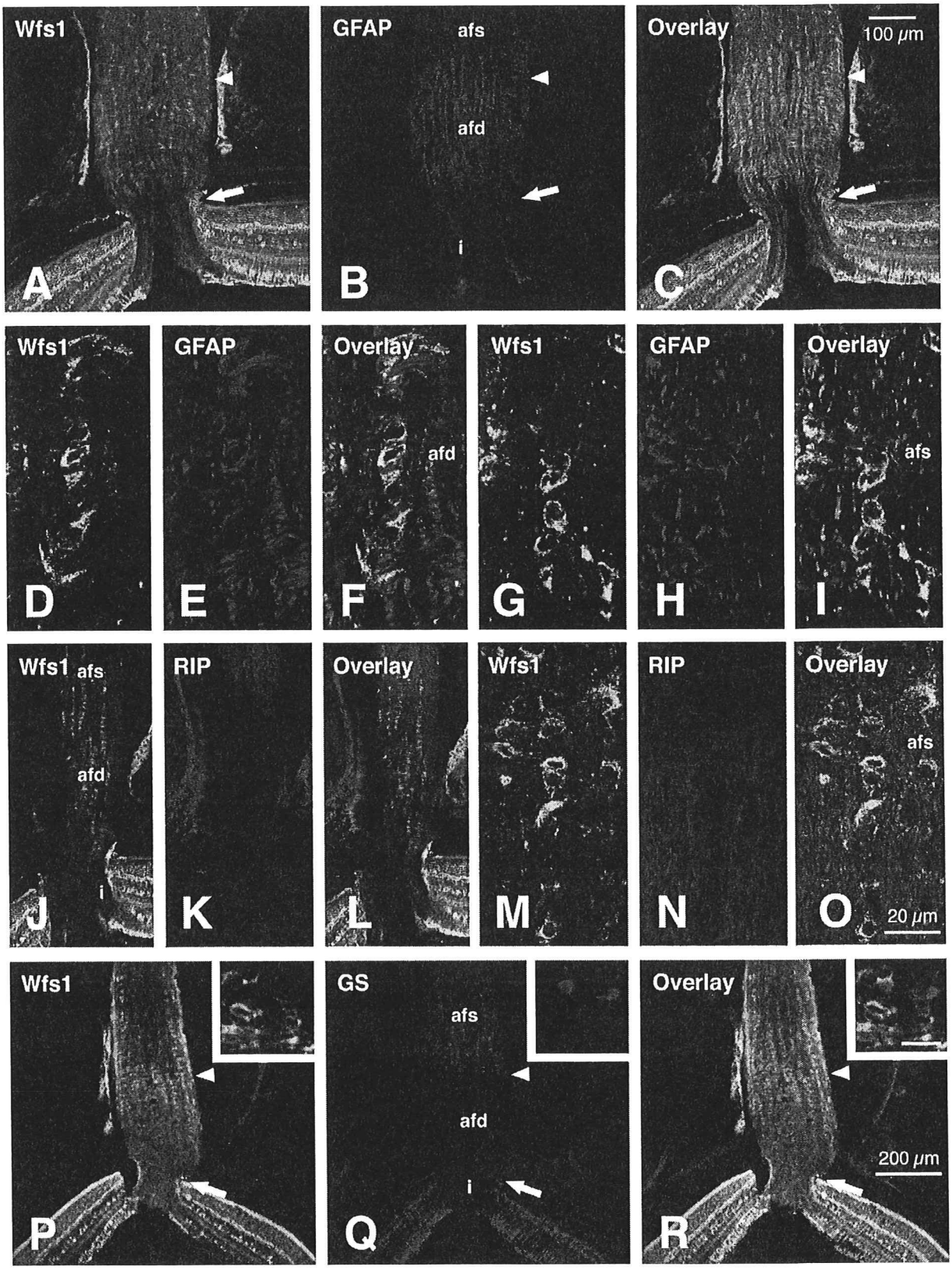
Wfs1
GFAP
afs
afd
i
Overlay
100 μm
A
B
C
Wfs1
GFAP
Overlay
afd
Wfs1
GFAP
Overlay
afs
D
E
F
G
H
I
Wfs1
afs
afd
i
RIP
Overlay
Wfs1
RIP
Overlay
afs
20 μm
J
K
L
M
N
O
Wfs1
GS
afs
afd
i
Overlay
200 μm
P
Q
R

Figure 8

TABLE 3. Distribution of Wfs1 Immunoreactivity in the Normal Mouse Optic Nerve

Optic Nerve Cells	
Astrocytes	+
Oligodendrocytes	–
Microglia	–

+, present; –, not present.

9E,F). Extremely weak or no immunoreactivity was seen in the optic chiasm, the optic tract, the LGN, the pretectum, and in the medial terminal nucleus (Fig. 10C,D; Table 4). When a normal rabbit immunoglobulin was used instead of the anti-Wfs1 antibody, no immunoreactivity was seen in the visual cortex, the SCN, and in the SC (data not shown). When the antibody preabsorbed by incubation with the GST-Wfs1N chimeric protein (antigen), immunoreactivity was not observed in these structures (Fig. 10B, data not shown).

DISCUSSION

We determined the expression pattern of the *Wfs1* gene in the normal mouse retina, optic nerve, SC, SCN, and in the visual cortex, at both the mRNA and protein levels. In these structures, not only neurons but also glial cells expressed Wfs1. In the retina, Wfs1 was expressed in all neuron types: photoreceptors, horizontal cells, bipolar cells, displaced (ON) and nondisplaced (OFF) amacrine cells, and RGCs. Müller glial cells also expressed Wfs1. In the optic nerve astrocytes were the site of Wfs1 expression. In the brain, Wfs1 was expressed in the zonal, superficial gray, and intermediate gray layers of the SC, in the dorsomedial part of the SCN, and in layer II of the primary and secondary visual cortical areas.

Specificity of anti-Wfs1 antibody

In the immunoblot analysis, the anti-Wfs1 antibody clearly recognized a single ≈100 kDa protein band of extracts from the brain and optic nerve (Fig. 1). The band size was consistent with an apparent molecular mass of ≈100 kDa that was examined in extracts from rodent brains (Takeda et al., 2001; Ishihara et al., 2004). This protein band disappeared when the antibody was preincubated with the antigen (GST-Wfs1N chimeric protein) (antibody-absorption experiment) (Fig. 1). Thus, the specificity of the antibody has been characterized in the mouse optic nerve as well as in the brain.

In the immunoblot analysis of retinal extracts the antibody detected both ≈100 kDa and ≈70 kDa bands. As for the ≈70 kDa Wfs1-immunoreactive band, a few reports have appeared. It is not known which kind of protein around ≈70 kDa the antibody detected. If the protein of this band is a part of the Wfs1 protein the appearance of the band likely resulted from degradation of the Wfs1 protein or from an alternative RNA splicing of the *Wfs1* gene in retinal cells. Since not only the ≈100 kDa band but also the ≈70 kDa band disappeared in the antibody-absorption experiment, the protein of ≈70 kDa is most probably a part of the Wfs1 protein containing a portion of the N-terminus antigen site (amino acids 1–179), that is, the antibody can be regarded as Wfs1-specific in the retina. However, there is a remote possibility that the anti-Wfs1 antibody detected a protein at ≈70 kDa other than Wfs1. This possibility will be verified by the immunoblot analysis of retinal extracts from *Wfs1* knockout mice, and by in situ hybridization histochemistry in retinal sections of the normal mouse.

Differences in localization of *Wfs1* expression between the mRNA and protein

There are clear differences in the localization of *Wfs1* expression between the mRNA and protein. In the retina, *Wfs1* mRNA was expressed in the ONL, INL, and GCL where cell bodies are concentrated, while Wfs1 protein was expressed not only in the ONL, INL, and GCL, but also in the OPL and IPL, where processes of retinal cells are accumulated (Fig. 2). Similar differences were also observed in the CA1 field of the hippocampus. In this region, *Wfs1* mRNA expression was confined to the pyramidal cell layer where cell bodies of pyramidal neurons are located, while Wfs1 protein was present not only in the pyramidal cell layer but also in the three strata (strata radiatum, lacunosum-moleculare, and oriens) where processes of pyramidal neurons are extended (Fig. 9A–C). Since the specificity of the anti-Wfs1 antibody in the CA1 field was strictly verified by the immunoblot analysis (present study) and by using *Wfs1* knockout mice (Ishihara et al., 2004), it is reasonable to speculate that the differences are not attributable to a nonspecific immunoreaction of the antibody, but to divergence in the localization of *Wfs1* expression between the mRNA and protein. In the retina, Wfs1 was expressed in all neuron types (photoreceptors, horizontal cells, bipolar cells, nondisplaced and displaced amacrine cells, and RGCs), and in Müller cells. Cell bodies of these cells are confined to the ONL, INL, and to GCL, and *Wfs1* mRNA expression was also confined to these layers. Therefore, there is little discrepancy in the localization of *Wfs1* expression between the mRNA and protein.

In addition, a neurobiological study reported that Wfs1 protein in the brain is found at higher steady-state levels than expected from the relatively low amount of *Wfs1* mRNA (Hofmann et al., 2003). Based on this evi-

Fig. 8. Cellular localization of Wfs1 in the normal mouse optic nerve. **A–I:** Double immunostaining for Wfs1 (Wfs1; A,D,G; Alexa Fluor 488 label; green) and for an astrocyte marker (glial fibrillary acidic protein, GFAP; B,E,H; Alexa Fluor 594 label; red). Cell nuclei are labeled in blue with bisBenzimide (Hoechst 33258). C,F,I are overlaid images. Arrows and arrowheads in A–C indicate the border between intraretinal (i) and astrocytic filament dense (afd) parts, and the boundary between the afd and astrocytic filament sparse (afs) parts, respectively. D–F,G–I are higher-magnification photomicrographs of the afd and afs parts, respectively. These panels show that Wfs1 immunoreactivity is observed in astrocytes. **J–O:** Double immunostaining for Wfs1 (Wfs1; J,M; Alexa Fluor 488 label; green) and for an oligodendrocyte marker (RIP; K,N; Alexa Fluor 594 label; red). Cell nuclei are labeled in blue with bisBenzimide (Hoechst 33258). L,O are overlaid images. M–O are higher-magnification photomicrographs of the afs part. These panels show that Wfs1 immunoreactivity is not seen in oligodendrocytes. **P–R:** Double immunostaining for Wfs1 (Wfs1; P; Alexa Fluor 488 label; green) and for a glial cell marker (glutamine synthetase, GS; Q; Alexa Fluor 594 label; red). R is an overlaid image. Arrows and arrowheads indicate the border between i and afd parts, and the boundary between the afd and afs parts, respectively. Insets are higher-magnification photomicrographs around the boundary between the afd and afs parts. These panels and insets show that colocalization of Wfs1 immunoreactivity and GS immunoreactivity is not seen in the optic nerve but in the retina. These fluorescence photomicrographs were taken with FV500 (Olympus; A–O), and with LSM 510 (Carl Zeiss; P–R) confocal microscopes. Scale bars = 100 μm in C applies to A,B, J–L; 20 μm in O applies to D–I, M,N; 200 μm in R applies to P–Q; 20 μm in inset of R applies to insets of P–Q.

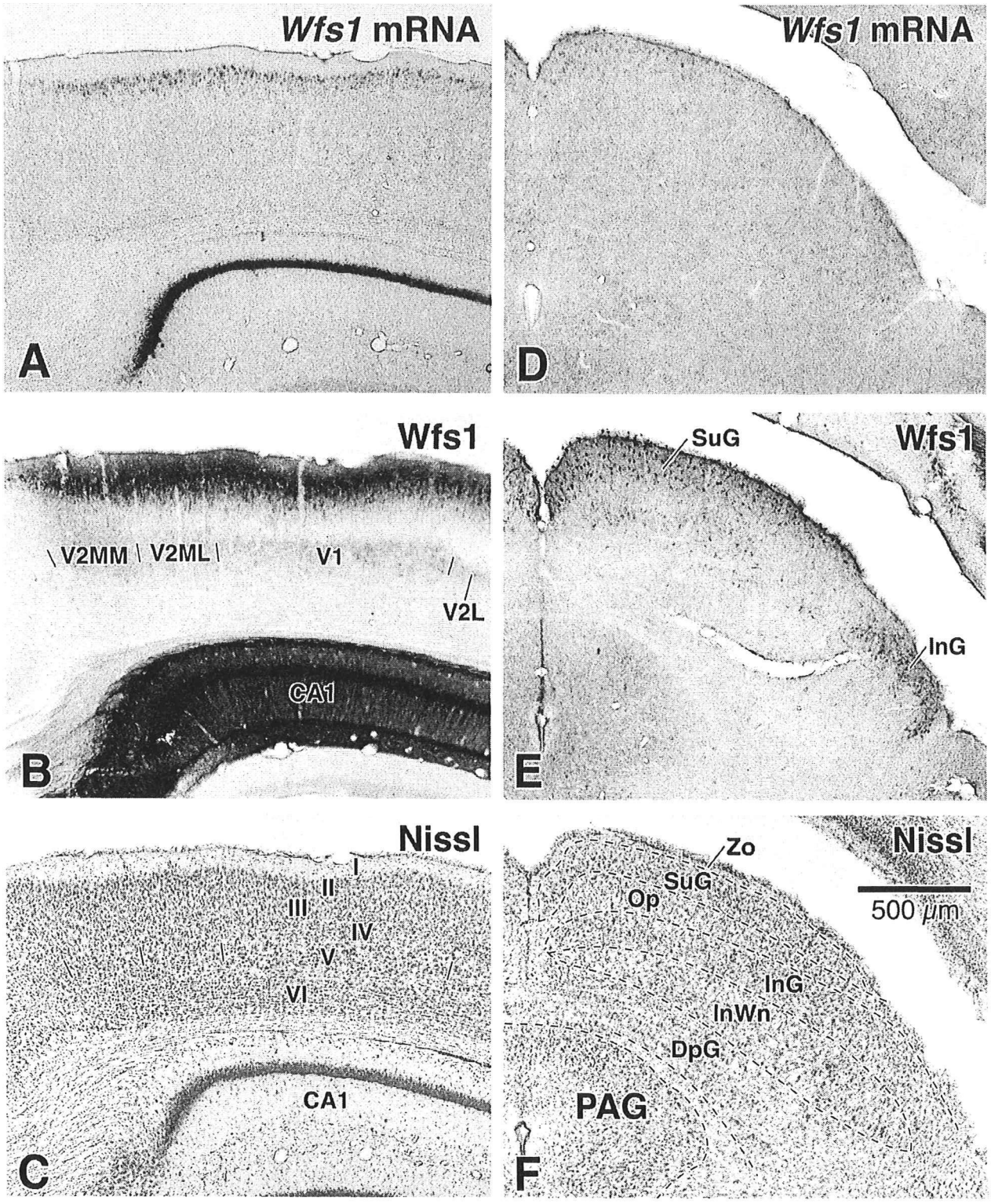

Fig. 9. *Wfs1* mRNA signals and protein immunoreactivity in the normal mouse brain. **A–C:** Mouse *Wfs1* mRNA signals (*Wfs1* mRNA; A), mouse Wfs1 protein immunoreactivity (Wfs1; B), and cytoarchitecture (Nissl; C) in three serial sections of the visual cortex hybridized with antisense cRNA probes of the mouse *Wfs1* 5′-terminus, immunostained with rabbit antimouse Wfs1 N-terminus antibody, and Nissl-stained with cresyl violet, respectively. Short lines in B,C indicate borders between each cortical area. These panels show that both *Wfs1* mRNA signals and Wfs1 immunoreactivity are observed in layer II of the visual cortex. V1, primary visual cortex; V2L, lateral area of the secondary visual cortex; V2ML, mediolateral area of the secondary visual cortex; V2MM, mediomedial area of the secondary visual cortex; CA1, CA1 field of the hippocampus; I, layer I; II, layer II; III, layer III; IV, layer IV; V, layer V; VI, layer VI. **D–F:** Mouse *Wfs1* mRNA signals (*Wfs1* mRNA; D), mouse Wfs1 protein immunoreactivity (Wfs1; E), and cytoarchitecture (Nissl; F) in three serial sections of the superior colliculus (SC). Dashed lines in F indicate borders of each superior collicular layer and the boundary of the periaqueductal gray (PAG). These panels show that *Wfs1* mRNA signals and Wfs1 immunoreactivity are seen in the zonal (Zo), superficial gray (SuG), and intermediate gray (InG) layers of the SC. Op, optic nerve layer of the SC; InWh, intermediate white layer of the SC; DpG, deep gray layer of the SC. Scale bar = 500 μm in F applies to A–E.

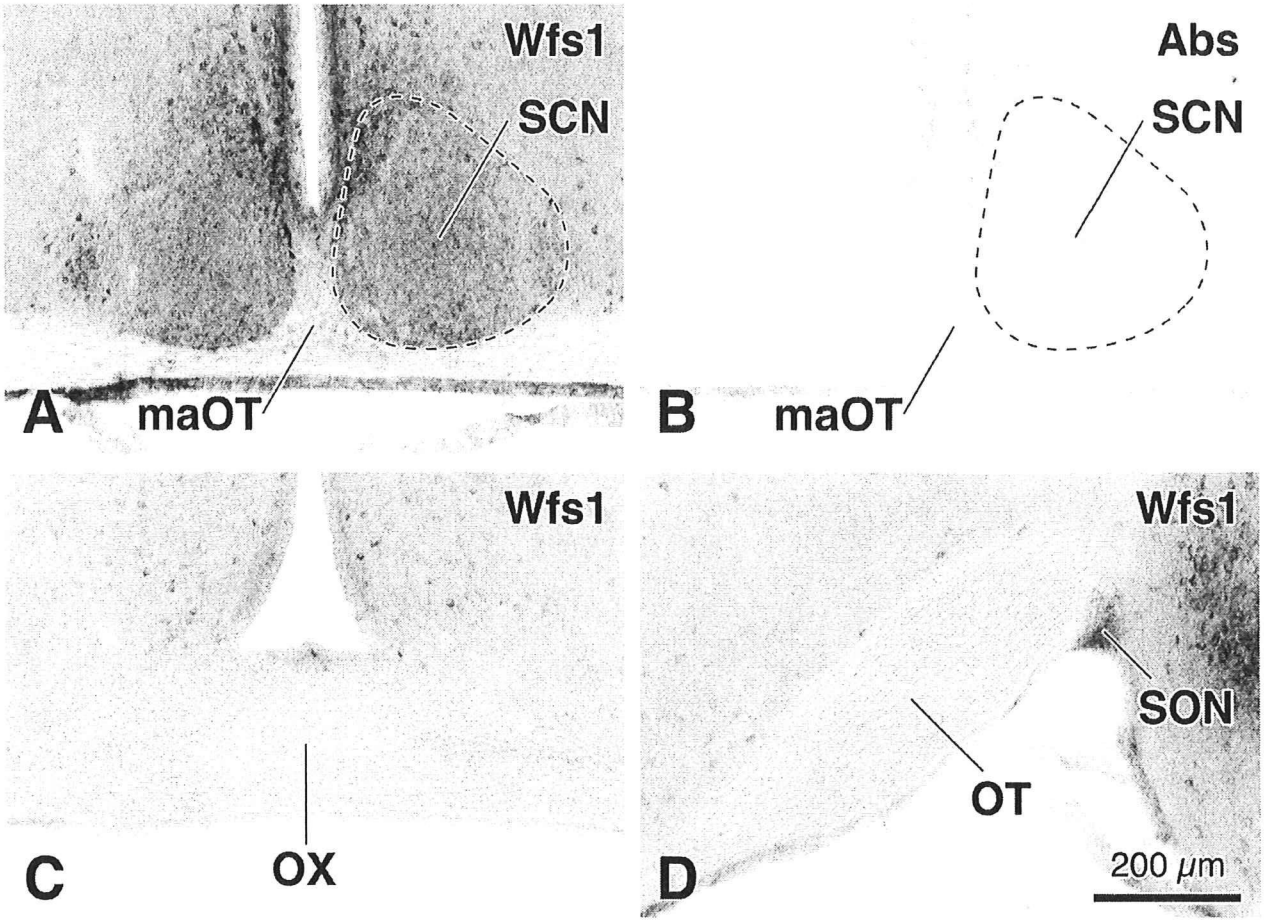

Fig. 10. Wfs1 protein immunoreactivity in the normal mouse suprachiasmatic nucleus (SCN), optic chiasm (OX), and optic tract (OT). **A,B:** Mouse Wfs1 protein immunoreactivity in two adjacent sections of the SCN immunostained with rabbit anti-Wfs1 N-terminus antibody (Wfs1; A), and with the antibody preabsorbed by incubation with GST-Wfs1 N-terminus chimeric protein (antigen) (Abs; B). The dashed lines indicate the boundary of the SCN. These panels show that moderate Wfs1 immunoreactivity is seen in the SCN. maOT, medial accessory optic tract. **C,D:** Mouse Wfs1 protein immunoreactivity in the OX (C) and OT (D). These panels show that Wfs1 immunoreactivity is not seen in the OX or OT. SON, supraoptic nucleus. Scale bar = 200 μm in D applies to A–C.

TABLE 4. Distribution of Wfs1 Immunoreactivity in the Normal Mouse Vision-Related Brain Structures

Vision-Related Brain Structures	
Optic chiasm	–
Optic tract	–
Suprachiasmatic nucleus	+
Lateral geniculate nucleus	–
Pretectum	–
Superior colliculus	+
Medial terminal nucleus	–
Primary visual cortex	+
Secondary visual cortex	+

+, present; –, not present.

dence it is reasonable to accept that the *Wfs1* mRNA expression is weaker than the protein expression in the retina. Therefore, results obtained achieve a reconciliation between *Wfs1* mRNA and protein expression in the retina.

Comparison with previous findings

Yamamoto et al. (2006) showed strong WFS1 immunolabeling in RGCs and optic nerve glial cells of the cynomolgus monkey. In the mouse, Wfs1 was expressed not only in RGCs but also in photoreceptors, horizontal cells, bipolar cells, amacrine cells, and in Müller cells of the retina. In the optic nerve, Wfs1 was present solely in astrocytes. In the brain, Takeda et al. (2001) described Wfs1 expression in layer II of the rat visual cortex. In the mouse, Wfs1 was expressed in the SC and SCN as well as in layer II of the visual cortex. These findings indicate that Wfs1 expression in RGCs, optic nerve glial cells, and in layer II of the visual cortex is similar among various mammalian species.

Retina

Photoreceptors. As for *Wfs1* mRNA expression in the inner segment, verification is necessary, since the inner segment is not a common site of mRNA accumulation. Results obtained clearly showed that *Wfs1* mRNA signals detected by antisense probes were much stronger than

those detected by sense probes (Fig. 2A,B). In addition, several histochemical studies have reported the distribution of mRNA signals in the inner segment (Bumsted et al., 1997; Cowlen et al., 2003; Nogami et al., 2006; Acar et al., 2007). Thus, it is reasonable to speculate that *Wfs1* mRNA is present in the inner segment.

Wfs1 protein immunoreactivity was observed in a majority of cell bodies in the ONL (Fig. 2C). Since rods make up 97.2% and cones 2.8% of all the photoreceptors in the C57 mouse retina (Jeon et al., 1998), the results obtained suggest that Wfs1 is expressed at least in rods. We also demonstrated that both *Wfs1* mRNA and protein were expressed in the inner segments and cell bodies of photoreceptors. Since Wfs1 was not expressed in the outer segments, it is possible that Wfs1 is not directly involved in phototransduction proper in this segment. Instead, Wfs1 is probably distributed as an ER membrane protein in the inner segments and cell bodies of photoreceptors (Takeda et al., 2001; Hofmann et al., 2003), and is considered responsible for the maintenance of phototransduction. In addition, slight photoreceptor dysfunction is suspected in Wolfram syndrome patients (Yamamoto et al., 2006), since the subjective dark adaptation curve in Wolfram syndrome patients shows a diminution of both cone and rod adaptation (Mtanda et al., 1986).

Horizontal cells. Since Wfs1-immunoreactive horizontal cells were calbindin-D-28K positive, Wfs1 was expressed at least in the axon-bearing type (Haverkamp and Wässle, 2000). This evidence indicates for the first time a possible role for this cell type in the pathologic course of Wolfram syndrome. In Wolfram syndrome patients low visual acuity and color visual disturbance are observed (Mtanda et al., 1986; Bitoun, 1994; Seynaeve et al., 1994; Barrett et al., 1997). According to a review by Wässle (2004), horizontal cell dendrites are inserted as lateral elements into the invaginating contacts of cone pedicles, and horizontal cell axon terminals form the lateral elements within rod spherules. Traditionally, it is assumed that horizontal cells release the inhibitory transmitter GABA (γ-aminobutyric acid) and provide feedback inhibition at the photoreceptor synaptic terminal. As horizontal cells summate light signals from several cones, such feedback would cause lateral inhibition, through which a cone's light response is reduced by the illumination of neighboring cones. This mechanism is thought to enhance the response to the edges of visual stimuli and to reduce the response to areas of uniform brightness (Wässle, 2004). Horizontal cell feedback in fish and turtle retinae seems to be cone-specific. However, no such chromatic organization of horizontal cell feedback has been observed in the primate retina, including the human retina (Dacey et al., 1996; Wässle, 2004). Thus, dysfunction of WFS1 protein in horizontal cells might be involved in the low visual acuity in Wolfram syndrome patients rather than color visual disturbance.

Bipolar cells. The Wfs1 immunoreactivity in rod and ON-cone bipolar cells is reliable for the following reasons. Wfs1/Goα double-labeled cells were observed in both the intermediate row of the INL (where cone bipolar cells are distributed) and in the outer row of the INL (where rod bipolar cells are located) (Haverkamp and Wässle, 2000). The immunoreactivity was verified by absorption experiments (Fig. 3G–I). Finally, certainty of the immunoreactivity was also supported by the weak *Wfs1* mRNA signals in the outer and intermediate rows of the INL (Fig. 2A,B).

Wfs1 immunoreactivity in OFF-cone bipolar cells was not examined in the present study. Markers for OFF-cone bipolar cells offered by Haverkamp and Wässle (2000) are Pep19, recoverin, glutamate transporter 1 (GLT-1), and caldendrin. In their study, all antibodies against these marker proteins were generated by a rabbit (Haverkamp and Wässle, 2000). Unfortunately, the anti-Wfs1 antibody was also generated by a rabbit, and the antibody produced perikaryon staining as the antibodies against the marker proteins did (Haverkamp and Wässle, 2000). To examine Wfs1 expression in the OFF-cone bipolar cells it is necessary to obtain other OFF-cone bipolar cell-specific antibodies generated by an animal other than the rabbit.

Amacrine cells. Strong Wfs1 expression was present in cholinergic amacrine cells (Figs. 3J–K, 4A–F). These cholinergic amacrine cells are starburst amacrine cells (Jeon et al., 1998), occurring as matching pairs of displaced (ON) and nondisplaced (OFF) amacrine cells, and their dendrites form two narrow strata in the IPL (Fig. 3K; Haverkamp and Wässle, 2000). It is known that cholinergic amacrine cells are a key element of the direction-selective circuitry. It is likely that both presynaptic and postsynaptic mechanisms are involved in the generation of direction-selective light responses (Yoshida et al., 2001; Euler et al., 2002; Fried et al., 2002; Taylor and Vaney, 2002, 2003; Wässle, 2004). Thus, dysfunction of WFS1 protein in cholinergic amacrine cells might contribute to the disturbance of direction-selective light responses in Wolfram syndrome patients.

RGCs (retinal ganglion cells). Since RGCs make up only 41% of all the neurons in the GCL of the C57 mouse retina (Jeon et al., 1998), we carefully examined Wfs1 expression in RGCs by Wfs1/tracer double labeling and by Wfs1/retinal ganglion cell-specific-marker double immunohistochemistry. Wfs1 expression in RGCs is reliable for the following reasons. Wfs1 expression was detected in RGCs retrogradely labeled with Fluorescent Latex Microspheres (Fig. 4G–I) or with Fluoro-Ruby (Fig. 5A–C), and the expression was verified by the control (preabsorption) experiments (Fig. 4J–L). Wfs1 expression was detected in RGCs immunolabeled with retinal ganglion cell markers: tubulin, βIII isoform, and Brn-3a (Fig. 4M–R). Noncholinergic but Wfs1-immunoreactive cells were distributed in the GCL (Fig. 4A–F). Probably most of these cells are Wfs1-immunoreactive ganglion cells, since the majority of displaced amacrine cells are cholinergic (Voigt, 1986; Brecha et al., 1988; Haverkamp and Wässle, 2000). Finally, the majority of calbindin-D-28K immunolabeled cells in the GCL were double-labeled with Wfs1 (Fig. 3M–O). A proportion of these Wfs1/calbindin-D-28K double-labeled cells are RGCs, since calbindin-D-28K is a marker for both RGCs and displaced amacrine cells in the GCL (Haverkamp and Wässle, 2000). Thus, Wfs1 is present in RGCs as well as in displaced amacrine cells in the GCL.

It is not well known which types of RGCs express Wfs1. Figure 4P–R shows that Wfs1 immunoreactivity is detected in both strongly and weakly Brn-3a-immunolabeled ganglion cells. Since Brn-3a is expressed at high levels in small ganglion cells but not in large ganglion cells, it is possible that Wfs1 is expressed in both small and large ganglion cells (Xiang et al., 1995; Haverkamp and Wässle, 2000).

IPL (inner plexiform layer). The mouse IPL is subdivided into five sublayers of equal thickness. These sublayers can be easily defined by immunolabeling the retina

for the calcium-binding proteins calbindin and calretinin, which shows three strongly labeled horizontal strata of processes (Fig. 3N; Haverkamp and Wässle, 2000; Wässle, 2004). Since the three Wfs1-immunoreactive strata in the IPL corresponded to those immunoreactive for the calcium-binding proteins (Fig. 3M–O), Wfs1 can be used as a marker for the three strongly labeled horizontal strata. In addition, the three strata contain Wfs1-immunoreactive processes of calbindin-D-28K-labeled amacrine and ganglion cells (Fig. 3M–O), since calbindin-D-28K is a marker for both amacrine and ganglion cells (Haverkamp and Wässle, 2000). Of these strata, the inner and outer strata also contain Wfs1-immunoreactive processes of cholinergic amacrine cells, since the two strata were immunoreactive for ChAT (Fig. 3J–L; Haverkamp and Wässle, 2000).

According to a review by Wässle (2004), the outer stratum contains the processes of the OFF-cholinergic amacrine cells, the dendrites of OFF-alpha cells, and the outer dendritic branches of direction selective cells. This band is densely packed with synapses and $GABA_A$ receptors (Brandstätter et al., 1995), and is where transient light responses and OFF direction-selective responses are calculated (Roska and Werblin, 2001). The intermediate stratum separates the OFF sublamina (outer) from the ON sublamina (inner). The polyaxonal amacrine cells (Ölveczky et al., 2003) ramify in this band, as do two GABA-containing amacrine cells. These cells contain, as well as GABA, a neuromodulator (nitric oxide and a catecholamine, respectively). Their functions are unknown. The inner stratum contains the axon terminals of an ON bipolar cell (Brown and Masland, 1999), the processes of the ON-cholinergic amacrine cells, the dendrites of ON-alpha cells, and the inner dendritic branches of direction-selective cells. This stratum is also densely packed with synapses and $GABA_A$ receptors, providing the circuitry for ON-transient light responses and ON direction-selective responses (Wässle, 2004). Thus, it is speculated that the inner stratum contains Wfs1-immunoreactive processes of bipolar cells, as well as those of amacrine and ganglion cells.

Müller cells. Wfs1 protein was expressed strongly in endfeet of Müller cells, moderately in internal radial processes, and weakly in cell bodies, whereas *Wfs1* mRNA signals were weak in the middle row of the INL where cell bodies of Müller cells are located. These results suggest that the turnover of Wfs1 protein in Müller cells is slower than that in other Wfs1-positive retinal neurons. As described above, Wfs1 protein was distributed densely in the endfeet of Müller cells, but sparsely in cell bodies. This evidence indicates that Wfs1 protein accumulates in the endfeet of Müller cells. Elucidating the cause of this accumulation might provide a clue as to the biochemical function of Wfs1 in glial cells including Müller cells.

Although Wolfram syndrome patients often develop diabetes mellitus early on (median age 6 years, range 3 weeks to 16 years; Barrett et al., 1997), they rarely develop diabetic retinopathy (Mtanda et al., 1986; Bitoun, 1994; Seynaeve et al., 1994; Barrett et al., 1997). Diabetic retinopathy is accompanied by a proliferation of new retinal vessels under hypoxic conditions. The proliferation is mediated by Müller cells via the release of vascular endothelial growth factor (VEGF) and transforming growth factor β or via direct contact with endothelial cells (Bringmann and Reichenbach, 2001). In Wolfram syndrome patients it is suggested that the functions of Müller cells are disrupted by loss-of-function mutations in the *WFS1* gene. Thus, the proliferation of new retinal vessels might be hampered by dysfunctional Müller cells in Wolfram syndrome patients.

Optic nerve

Mice lack intraretinal myelination and a well-developed lamina cribrosa but exhibit a marked concentration of astrocytic filaments at the retinal optic nerve junction (Morcos and Chan-Ling, 2000). Based on this evidence, we divided the mouse optic nerve into three parts (i, afd, and afs) defined by the position of the sensory retina and by the distribution of astrocytic filaments. These criteria for the optic nerve subdivisions are appropriate since the distribution of GS-positive cells corresponded to the afs part. Thus, mouse optic nerve is also divided into three parts by the position of the sensory retina and by the distribution of GS-positive cells as shown in Figure 8Q.

Wfs1-positive astrocytes were distributed in the optic nerve, but not in the retina, optic chiasm, or optic tract (Figs. 8A–I, 10C,D). This evidence suggests that the astrocytes in the optic nerve are different from those in the retina, optic chiasm, and optic tract. Further studies are required to clarify the morphological and functional differences between Wfs1-positive astrocytes in the optic nerve and Wfs1-negative astrocytes in the optic chiasm and the optic tract. These studies could provide valuable insights into the physiological role of Wfs1 protein in astrocytes.

Vision-related brain structures

Superior colliculus. The superficial gray layer receives visual inputs directly from the retina and occipital cortex and contains cells that project extrinsically to dorsal thalamic nuclei (Edwards et al., 1986), whereas the intermediate gray layer receives indirect retinal inputs by way of the lateral division of the ventral lateral geniculate nucleus (Brauer and Schober, 1982). Wfs1-positive neurons in the intermediate gray layer as well as those in the superficial gray layer might be involved in visual functions. Neuropathological studies have demonstrated neuronal loss and gliosis in the SC of Wolfram syndrome patients (Genís et al., 1997; Shannon et al., 1999). These findings might be attributed to dysfunctional SC neurons in Wolfram syndrome patients due to loss-of-function mutations in the *WFS1* gene.

Suprachiasmatic nucleus. The SCN is a circadian pacemaker. In the SCN, Wfs1-positive neurons were distributed in the dorsomedial region. This region does not receive direct retinal inputs, but does receive inputs from nonvisual sources. The region sends large numbers of axons to the hypothalamus and small numbers of axons to the thalamus, including the paraventricular thalamic nucleus (PVT). In the PVT, circadian timing information from the SCN is conveyed to multiple limbic structures including the amygdala and the limbic cortical areas (Watts and Swanson, 1987; Kawano et al., 2001; Leak and Moore, 2001). Thus, it is speculated that Wfs1-positive neurons in the dorsomedial part of the SCN provide circadian timing cues to the hypothalamus, the thalamus, and even to the multiple limbic structures without receiving direct retinal inputs.

Visual cortex. The laminar distribution of Wfs1-positive neurons in layer II was present throughout the

mouse neocortex (Kawano et al., unpubl. obs.), as described in the rat (Takeda et al., 2001). Therefore, the distribution is not restricted to the visual cortex. Few thalamic afferents to the visual cortex terminate in layer II (afferents to V1 principally arise in the dorsal lateral geniculate nucleus; Peters and Feldman, 1976; afferents to V2 mainly arise in the lateral posterior nucleus; Olavarria, 1979), but associational afferents from other visual cortical areas terminate in layer II (Coogan and Burkhalter, 1990, 1993). Layer II neurons send associational fibers to the other visual cortical areas (Miller and Vogt, 1984a; Sanderson et al., 1991). Apart from the associational connections, the commissural neurons and terminals are concentrated in a narrow region (the border between V1 and V2L) where the vertical meridian is represented (Cipolloni and Peters, 1979; Cusick and Lund, 1981). In this region, layer II neurons send commissural fibers to and receive commissural fibers from the opposite cortex (Miller and Vogt, 1984b; Sefton et al., 1991). In addition, local circuit neurons are also located in layer II. These neurons make widespread connections within the same layer and project strongly to layer V (Burkhalter, 1989; Sefton and Dreher, 1995). Therefore, Wfs1-immunoreactive punctuations in layer V might be attributed to the strong projections from Wfs1-positive neurons in layer II to layer V. Further studies using tract-tracing methods are required to clarify the fiber connections of Wfs1-positive neurons in layer II. Neuroradiological and neuropathological studies have shown that there is mild cerebrocortical atrophy in Wolfram syndrome patients (Rando et al., 1992; Scolding et al., 1996; Shannon et al., 1999). The atrophy might be attributed to the dysfunctional cortical layer II neurons in Wolfram syndrome patients resulting from loss-of-function mutations in the *WFS1* gene.

Optic atrophy

Optic atrophy is one of the minimal diagnostic criteria for Wolfram syndrome (Barrett et al., 1997). In this section we discuss the pathogenesis of optic atrophy in Wolfram syndrome based on the results obtained. Wfs1 was expressed in all neuron types (RGCs, amacrine cells, bipolar cells, horizontal cells, and photoreceptors) and Müller cells of the retina, in astrocytes of the optic nerve, and in neurons of the SC and the SCN. Out of these cells, candidates for causative cells for optic atrophy in Wolfram syndrome are not only RGCs but also amacrine cells, bipolar cells, SC neurons, SCN neurons, Müller cells, and astrocytes in the optic nerve, since it is speculated that candidate neurons express Wfs1 and are directly connected with RGCs and that cell bodies or axons of RGCs are surrounded by candidate glial cells.

First, we discuss whether RGCs are the principal candidates. In this case, autosomal dominant optic atrophy (ADOA) is useful for comparisons with Wolfram syndrome. ADOA is one of the primary inherited optic neuropathies, and has been attributed to mutations in the *OPA1* gene (Alexander et al., 2000; Delettre et al., 2000; Votruba et al., 2003). OPA1 protein expression is present in RGCs in the mouse, rat, and human (Aijaz et al., 2004; Pesch et al., 2004; Ju et al., 2005). The pattern electroretinogram (PERG) in ADOA patients shows an abnormal N95:P50 ratio, with a reduction in the amplitude of the N95 waveform (Berninger et al., 1991; Holder et al., 1998). Since the PERG N95 component is postulated to be specific for the retinal ganglion cell (Ryan and Arden, 1988), this finding supports a ganglion cell origin for ADOA (Votruba et al., 2003). By contrast, the ERG tests in Wolfram syndrome patients revealed normal or only slightly reduced responses, suggesting that the pathogenesis of the optic atrophy does not lie in the retina, but primarily affects the optic nerve (Niemeyer and Marquardt, 1972; Mtanda et al., 1986; Seynaeve et al., 1994; Barrett et al., 1997). In addition, Barrett et al. (1997) concluded that the reduced visual acuity not due to a refractive error and color vision defect suggested a site of pathology in the visual pathway proximal (posterior) to the eye. Thus, it is possible that the dysfunction of RGCs in Wolfram syndrome patients is mild and that the pathogenesis of optic atrophy is not attributable to the RGCs proper.

Previous clinical, pathological, and neurobiological studies weakly support the notion that amacrine cells, bipolar cells, SC neurons, SCN neurons, and Müller cells are the principal candidates. Although Wfs1 was expressed strongly in amacrine cells and weakly in bipolar cells, there have been few findings of functional abnormality in the INL of Wolfram syndrome patients by using ERGs (Niemeyer and Marquardt, 1972; Mtanda et al., 1986; Seynaeve et al., 1994; Barrett et al., 1997). In the mouse SC, Wfs1-positive cells were distributed in the superficial gray layer where retinal afferents terminate. In Wolfram syndrome patients, neuronal loss and gliosis are observed in the SC (Genís et al., 1997; Shannon et al., 1999). It is possible that optic atrophy is induced by retrograde degeneration of RGCs from the SC. In this case, the degenerated RGCs would be M-cells and K-cells (Y-cells and W-cells in the cat) not P-cells (X-cells in the cat; Garey, 1990; Goebel et al., 2004). By contrast, there is neuronal loss in the LGN mainly involving layers 3–6, which are P-cell relay layers (Garey, 1990; Genís et al., 1997; Goebel et al., 2004) or neuronal loss in all six layers of the LGN (Shannon et al., 1999). If SC neurons are the principal candidates, it is difficult to explain the loss of neurons in the LGN involving the P-cell relay layers. In the mouse SCN, Wfs1-positive neurons are distributed in the dorsomedial part where retinal afferents do not directly terminate. Since strong Wfs1 expression is present in Müller cells, and since RGCs are surrounded by Müller cells, there is a possibility that loss-of-function of Müller cells induces degeneration of RGCs in Wolfram syndrome patients. A neurobiological study using NSE-Hu-Bcl-2 transgenic mice demonstrated that early postnatal Müller cell death leads to retinal degeneration but not optic nerve degeneration (Dubois-Dauphin et al., 2000). It is improbable that Müller cells are the principal candidates. Thus, it is speculated that astrocytes in the optic nerve are the principal candidates for the causative cells for optic atrophy in Wolfram syndrome patients.

Since Wfs1 is expressed in many tissues, the reason why astrocytes in the optic nerve and not other cell types are principally affected by *WFS1* mutations which cause the optic atrophy in Wolfram syndrome is unknown. A biochemical study by using *Xenopus* oocytes suggested that WFS1 protein serves directly as a novel endoplasmic reticulum (ER) calcium channel or, alternatively, as a regulator of ER calcium channel activity. *WFS1* mutations associated with Wolfram syndrome reduce the susceptibility to cation block. It is possible that WFS1 protein-mediated regulation of intracellular calcium provides an important protective function in neurons and/or glial cells that are dependent on the ER for calcium signaling (Hay-

don, 2001; Osman et al., 2003). Recently, a functional study indicated that WFS1 protein expression increases in response to ER stress and that the protein plays a physiological role in protecting cells from ER stress-induced apoptosis (Ueda et al., 2005). Although the biochemical function of WFS1 in neurons and/or glial cells in the visual system remains to be investigated, it is possible that WFS1 mutations in the neurons and/or glial cells cause a disruption of the WFS1-mediated regulation of intracellular calcium levels and/or of the ER stress responses, and a consequent malfunction of electrophysiological activity in the neurons and/or glial cells (Haydon, 2001; Volterra and Meldolesi, 2005; Seifert et al., 2006). This loss-of-function may impair axons of RGCs leading to optic atrophy.

Wfs1 was localized to the afd part of the mouse optic nerve where GS immunoreactivity was almost negative (Figs. 6B, 8Q). This evidence suggests that a lack of GS in the afd part might augment the damage to the optic nerve caused by glutamate. Recently, vesicular glutamate release from axons was demonstrated not only in the corpus callosum but also in the optic nerve of rodents after the propagation of action potentials (Kukley et al., 2007; Ziskin et al., 2007). Thus, impaired glutamate clearance attributable to a lack of GS in the afd part may affect the viability of optic nerve axons in the mouse, including the *Wfs1* knockout mouse.

CONCLUSION

In summary, Wfs1 was present not only in RGCs but also in photoreceptors, horizontal cells, bipolar cells, amacrine cells, and Müller cells of the retina, in astrocytes of the optic nerve, and in neurons of the SC, the SCN, and of the visual cortex. Interestingly, Wfs1 was localized to the afd part of the optic nerve where GS immunoreactivity was almost negative. These results suggest that mutant WFS1 may contribute to the dysfunction of WFS1-expressing neurons and/or glial cells, which may in turn lead to optic atrophy in Wolfram syndrome. They also suggest that the lack of GS in the afd part might augment the damage to the optic nerve caused by glutamate. Although these notions are difficult to test experimentally, the availability of the Wfs1 mouse model could offer opportunities for further investigation. These studies are required to determine the exact physiological role of Wfs1 protein in the biology of vision and to obtain more insights into its pathophysiological roles in optic atrophy in Wolfram syndrome.

ACKNOWLEDGMENTS

The first and corresponding author, June Kawano, thanks Professor Shiro Nakagawa and Associate Professor Satoshi Kuchiiwa (Laboratory for Neuroanatomy, Department of Neurology, Kagoshima University Graduate School of Medical and Dental Sciences) for encouragement and for valuable discussions.

LITERATURE CITED

Acar N, Gregoire S, Andre A, Juaneda P, Joffre C, Bron AM, Creuzot-Garcher CP, Bretillon L. 2007. Plasmalogens in the retina: in situ hybridization of dihydroxyacetone phosphate acyltransferase (DHAP-AT)—the first enzyme involved in their biosynthesis—and comparative study of retinal and retinal pigment epithelial lipid composition. Exp Eye Res 84:143–151.

Aijaz S, Erskine L, Jeffery G, Bhattacharya SS, Votruba M. 2004. Developmental expression profile of the optic atrophy gene product: OPA1 is not localized exclusively in the mammalian retinal ganglion cell layer. Invest Ophthalmol Vis Sci 45:1667–1673.

Alexander C, Votruba M, Pesch UE, Thiselton DL, Mayer S, Moore A, Rodriguez M, Kellner U, Leo-Kottler B, Auburger G, Bhattacharya SS, Wissinger B. 2000. *OPA1*, encoding a dynamin-related GTPase, is mutated in autosomal dominant optic atrophy linked to chromosome 3q28. Nat Genet 26:211–215.

Barrett TG, Bundey SE, Macleod AF. 1995. Neurodegeneration and diabetes: UK nationwide study of Wolfram (DIDMOAD) syndrome. Lancet 346:1458–1463.

Barrett TG, Bundey SE, Fielder AR, Good PA. 1997. Optic atrophy in Wolfram (DIDMOAD) syndrome. Eye 11:882–888.

Berninger TA, Jaeger W, Krastel H. 1991. Electrophysiology and colour perimetry in dominant infantile optic atrophy. Br J Ophthalmol 75:49–52.

Bitoun P. 1994. Wolfram syndrome. A report of four cases and review of the literature. Ophthalmic Genet 15:77–85.

Brandstätter JH, Greferath U, Euler T, Wässle H. 1995. Co-stratification of $GABA_A$ receptors with the directionally selective circuitry of the rat retina. Vis Neurosci 12:345–358.

Brauer K, Schober W. 1982. Identification of geniculo-tectal relay neurons in the rat's ventral lateral geniculate nucleus. Exp Brain Res 45:84–88.

Brecha N, Johnson D, Peichl L, Wässle H. 1988. Cholinergic amacrine cells of the rabbit retina contain glutamate decarboxylase and g-aminobutyrate immunoreactivity. Proc Natl Acad Sci U S A 85:6187–6191.

Bringmann A, Reichenbach A. 2001. Role of Müller cells in retinal degenerations. Front Biosci 6:E72–92.

Brown SP, Masland RH. 1999. Costratification of a population of bipolar cells with the direction-selective circuitry of the rabbit retina. J Comp Neurol 408:97–106.

Bumsted K, Jasoni C, Szél A, Hendrickson A. 1997. Spatial and temporal expression of cone opsins during monkey retinal development. J Comp Neurol 378:117–134.

Burkhalter A. 1989. Intrinsic connections of rat primary visual cortex: laminar organization of axonal projections. J Comp Neurol 279:171–186.

Cipolloni PB, Peters A. 1979. The bilaminar and banded distribution of the callosal terminals in the posterior neocortex of the rat. Brain Res 176:33–47.

Collier DA, Barrett TG, Curtis D, Macleod A, Arranz MJ, Maassen JA, Bundey S. 1996. Linkage of Wolfram syndrome to chromosome 4p16.1 and evidence for heterogeneity. Am J Hum Genet 59:855–863.

Coogan TA, Burkhalter A. 1990. Conserved patterns of cortico-cortical connections define areal hierarchy in rat visual cortex. Exp Brain Res 80:49–53.

Coogan TA, Burkhalter A. 1993. Hierarchical organization of areas in rat visual cortex. J Neurosci 13:3749–3772.

Cowlen MS, Zhang VZ, Warnock L, Moyer CF, Peterson WM, Yerxa BR. 2003. Localization of ocular $P2Y_2$ receptor gene expression by in situ hybridization. Exp Eye Res 77:77–84.

Cryns K, Thys S, Van Laer L, Oka Y, Pfister M, Van Nassauw L, Smith RJ, Timmermans JP, Van Camp G. 2003. The *WFS1* gene, responsible for low frequency sensorineural hearing loss and Wolfram syndrome, is expressed in a variety of inner ear cells. Histochem Cell Biol 119:247–256.

Cusick CG, Lund RD. 1981. The distribution of the callosal projection to the occipital visual cortex in rats and mice. Brain Res 214:239–259.

Dacey DM, Lee BB, Stafford DK, Pokorny J, Smith VC. 1996. Horizontal cells of the primate retina: cone specificity without spectral opponency. Science 271:656–659.

Debus E, Weber K, Osborn M. 1983. Monoclonal antibodies specific for glial fibrillary acidic (GFA) protein and for each of the neurofilament triplet polypeptides. Differentiation 25:193–203.

Delettre C, Lenaers G, Griffoin JM, Gigarel N, Lorenzo C, Belenguer P, Pelloquin L, Grosgeorge J, Turc-Carel C, Perret E, Astarie-Dequeker C, Lasquellec L, Arnaud B, Ducommun B, Kaplan J, Hamel CP. 2000. Nuclear gene *OPA1*, encoding a mitochondrial dynamin-related protein, is mutated in dominant optic atrophy. Nat Genet 26:207–210.

Dráberová E, Lukás Z, Ivanyi D, Viklicky V, Dráber P. 1998. Expression of